

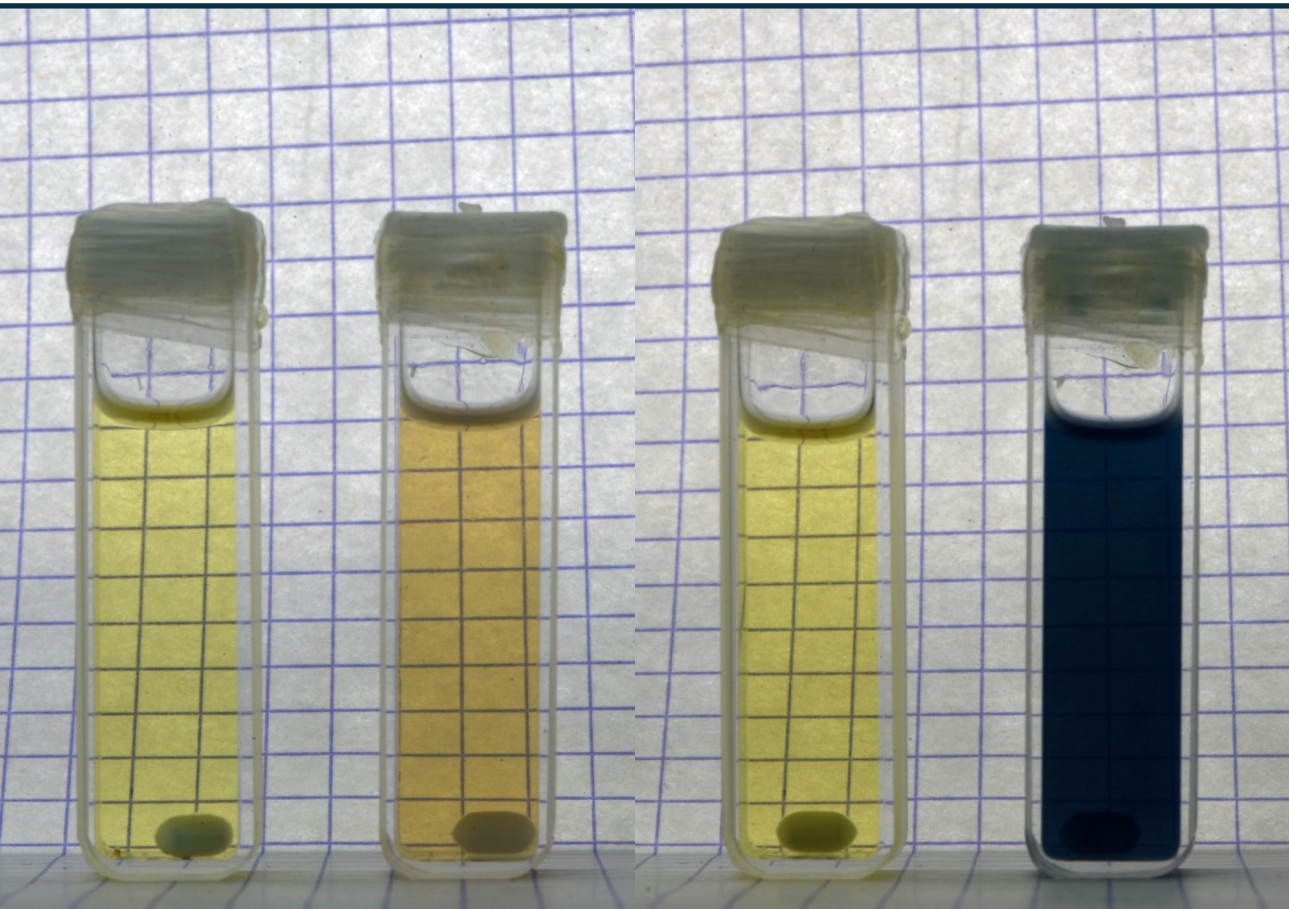


RIGA TECHNICAL
UNIVERSITY

Raivis Eglītis

PHOTOCHROMIC MATERIALS BASED ON ULTRA SMALL TITANIUM DIOXIDE NANOPARTICLES

Summary of the Doctoral Thesis



RIGA TECHNICAL UNIVERSITY
Faculty of Materials Science and Applied Chemistry
Institute of Materials and Surface Engineering

Raivis Eglītis

Doctoral Student of the Study Programme “Materials Science”

**Photochromic materials based on ultra small
titanium dioxide nanoparticles**

Summary of the Doctoral Thesis

Scientific supervisor
Professor Dr. sc. ing.
ANDRIS ŠUTKA

RTU Press
Riga 2023

Eglītis, R. Photochromic Materials Based on Ultra Small Titanium Dioxide Nanoparticles. Summary of the Doctoral Thesis. Riga: RTU Press, 2023. 51 p.

Published in accordance with the decision of the Promotion Council “RTU P-02” of 16 September 2022, Minutes No. 04030-9.2.2/10.

This work has been supported by the European Social Fund within the Project No 8.2.2.0/20/I/008 “Strengthening of PhD students and academic personnel of Riga Technical University and BA School of Business and Finance in the strategic fields of specialization” of the Specific Objective 8.2.2 “To Strengthen Academic Staff of Higher Education Institutions in Strategic Specialization Areas” of the Operational Programme “Growth and Employment”



NATIONAL
DEVELOPMENT
PLAN 2020



EUROPEAN UNION
European Social
Fund

INVESTING IN YOUR FUTURE

This publication was supported by Riga Technical University's Doctoral Grant programme

Cover photo by Raivis Eglītis

<https://doi.org/10.7250/9789934228636>

ISBN 978-9934-22-863-6 (pdf)

DOCTORAL THESIS PROPOSED TO RIGA TECHNICAL UNIVERSITY FOR THE PROMOTION TO THE SCIENTIFIC DEGREE OF DOCTOR OF SCIENCE

To be granted the scientific degree of Doctor of Science (Ph. D.), the present Doctoral Thesis has been submitted for the defence at the open meeting of RTU Promotion Council on 2 March 2023 at 10.30 at the Faculty of Materials Science and Applied Chemistry of Riga Technical University, 3 Paula Valdena Street, Room 272.

OFFICIAL REVIEWERS

Dr. chem. Donāts Erts
University of Latvia, Latvia

Dr. phys. Anatolijs Šarakovskis,
University of Latvia, Latvia

PhD. Gemma García Mandayo,
Centro de Estudios e Investigaciones Técnicas de Gipuzkoa, Spain

DECLARATION OF ACADEMIC INTEGRITY

I hereby declare that the Doctoral Thesis submitted for the review to Riga Technical University for the promotion to the scientific degree of Doctor of Science (Ph. D.) is my own. I confirm that this Doctoral Thesis had not been submitted to any other university for the promotion to a scientific degree.

Name Surname (signature)

Date:

The Doctoral Thesis has been written in English. It consists of an Introduction, 3 chapters, Conclusions, 79 figures, 4 tables; the total number of pages is 141. The Bibliography contains 376 titles.

Contents

List of abbreviations	5
1. Literature overview	10
2. Methods section	13
2.1. Synthesis of TiO ₂ and doped TiO ₂ nanoparticles	13
2.2. Determination of photochromic properties using UV-Vis spectroscopy	13
3. Results and Discussion	15
3.1. Photochromic properties of titanium dioxide	15
3.2. The electrical properties of titanium dioxide thin films under UV illumination and in the presence of hole scavenger vapors	19
3.3. Photoelectron accumulation in titanium dioxide films under UV irradiation while submersed in a hole scavenger	23
3.4. The influence of Nb ⁵⁺ dopant on photochromic response of titanium dioxide	25
3.5. Photochromic TiO ₂ polymer gels	35
3.6. Conclusions	46
References	48

LIST OF ABBREVIATIONS

HVAC	heating, ventilation, and cooling
ROS	reactive oxygen species
4-DDBSA	4-dodecylbenzene sulphonic acid
EtOH	ethanol
MeOH	methanol
<i>i</i> PrOH	isopropanol
<i>n</i> PrOH	<i>n</i> -propanol
<i>n</i> BuOH	<i>n</i> -butanol
<i>n</i> AmOH	<i>n</i> -pentanol
<i>n</i> HexOH	<i>n</i> -hexanol
MEOA	monoethanolamine
DEOA	diethanolamine
TEOA	triethanolamine
AcacH	acetylacetone
Acac	acetylacetonate ligand
(<i>n</i> BuO) ₄ Ti	tetra (<i>n</i> -butoxy) titanate
TiO ₂	titanium dioxide
CaH ₂	calcium hydride
Nb(OEt) ₅	niobium penta ethoxide
TMO	transition metal oxide
DMF	<i>N,N</i> -dimethylformamide
PEGDA	polyethylene glycol diacrylate
TCO	transparent conducting oxide
ITO	tin doped Indium oxide

ANNOTATION

Nowadays, global warming is causing a slow, but sure increase in the average annual temperature. This causes more countries to experience more and more extremely hot days. To be able to ensure comfortable working and living conditions in buildings, HVAC systems need to be used. However, these systems are power hungry and can account for around a third of the electrical energy consumption of buildings, especially office buildings. To reduce their usage, we need to reduce the amount of incoming light and with it – heat.

A slowly emerging technology are smart windows that can modulate the incoming light by dynamically changing their optical transmittance. The main technology behind smart windows are electrochromic materials, which change the optical properties when an electric field is applied. However, these require the usage of electricity and other constituents to ensure any autonomous action. Photochromic materials can act fully autonomously by changing their transmittance in response to incoming light.

The Thesis explores the photochromic properties of titanium dioxide nanoparticles in different environments. Furthermore, the modification of the nanoparticles with the introduction of a dopant cation and the influence on the photochromic properties is examined. Lastly, the electric properties of the nanoparticles were also examined. It was seen that the environment in which the nanoparticles are dispersed as well as the modification of the nanoparticles has a profound effect on the photochromic properties and can change not only the photodarkening kinetics but also the recovery kinetics. Furthermore, the incorporation of the nanoparticles into organic gels was achieved while retaining high transparency and the photochromic properties of the nanoparticles. Finally, it was shown that the photochromic process was accompanied by changes in the electric properties of the nanoparticles which were used to determine the amount of photoaccumulated electron carriers in the nanoparticles.

INTRODUCTION

Chromism is a material's change in color in response to an external stimulus. Chromic materials have become a staple of modern life in different ways – be it color changing thermometers, self-tinting glasses, or even smart windows. Out of the different types of chromism, photochromism stands out as being one of the most significant because of its passive nature and a wide range of applications. Furthermore, its combinations with other chromism types make it an important characteristic for any material.

In most cases the photochromic material used is organic. This means that its lifetime is limited. Conversely, although inorganic photochromic materials are also widely known, their usage is limited due to their (in most cases) relatively slow chromism. Furthermore, most of the inorganic photochromic materials are either classified as toxic, expensive, or scarce. Currently titanium dioxide does not have any of these drawbacks. However, its photochromic capabilities are not as well pronounced and are overshadowed by other materials, such as tungsten oxide. Although a material is usually looked at on its own, in most cases it is but a part of a larger system, meaning that its capabilities should be examined with respect to other components. Furthermore, it should be possible to offset the drawbacks of titanium dioxide with different methods, making it a more viable candidate for wide scale usage in photochromic applications. The term “ultra-small” refers to the fact that the size of nanoparticles are smaller than 10 nm. Furthermore, since photochromism is a surface process for nanoparticles, the usage of smaller nanoparticles leads to higher photodarkening and recovery speeds than for larger nanoparticles.

Aim of the Thesis

To synthesize ultra-small TiO₂ nanoparticles with high absorption and study their photochromic properties and incorporate them into a gel matrix.

Main tasks

- To study the influence of the surrounding medium on the photochromic properties of TiO₂ nanoparticles.
- To synthesize doped TiO₂ nanoparticles with a high amount of acceptor dopants (such as Nb⁵⁺).
- To study the photochromic properties of the synthesized doped TiO₂ nanoparticles.
- To incorporate TiO₂ nanoparticles into a polymer matrix while retaining high transparency to prepare photochromic gels capable of a high degree of light modulation.

Scientific significance

The influence of the hole scavenger as well as the dopant influence on the photochromic properties of TiO₂ are shown, indicating the possibility of severely influencing the photochromic properties. Furthermore, as of the performing this research, no transparent photochromic gels based on TiO₂ have been reported in literature.

Practical significance

Photochromic materials can be used to form smart windows that are capable of solar light modulation. This has the significance of providing a relatively inexpensive alternative to current smart window technologies employing mostly tungsten oxide or organic chromic materials. The incorporation of the photochromic nanoparticles in polymer gels would provide the

possibility of producing photochromic gel films based on stable inorganic photochromic materials.

Defendable theses

1. The photochromic properties of titanium dioxide are strongly related to its surrounding medium, given that photochromism is limited by the hole scavenging happening on the surface of the photochromic material.
2. The effect of photochromism on titanium dioxide is detectable not only by optical means but also by changes in the electric properties of the nanoparticles, as photochromism is accompanied by the photoaccumulation of electrons, which can change the electric properties of the material.
3. Doping of titanium dioxide with acceptor dopants has a strong positive influence on the photochromic properties of the material and increases the photodarkening rate.
4. It is possible to incorporate titanium dioxide into a transparent gel matrix while retaining the transmittance if the nanoparticles are small enough. This allows to obtain photochromic gels that are transparent in the un-darkened state.

APROBATION OF THE RESEARCH

Publications:

1. Eglītis, R., Šutka, A. Photochromic TiO₂/PEGDA organogels. *Photochem Photobiol Sci*, 2022. DOI: 10.1007/s43630-022-00183-6
2. Šutka, A., Eglītis, R., Kuzma, A., Smits, K., Zukuls, A., Prades, J.D., Fàbrega, C. Photodoping-Inspired Room-Temperature Gas Sensing by Anatase TiO₂ Quantum Dots. *ACS Applied Nano Materials*, 2021, 4, (3), pp. 2522–2527 DOI: 10.1021/acsanm.0c03089
3. Eglītis, R., Joost, U., Zukuls, A., Rubenis, K., Ignatāns, R., Avotiņa, L., Baumanė, L., Šmits, Krišjānis., Hirsimäki, M., Käämbre, T., Šutka, A. Strong, Rapid, and Reversible Photochromic Response of Nb Doped TiO₂ Nanocrystal Colloids in Hole Scavenging Media, *ACS Applied Materials & Interfaces*, 2020, 12 (51), 57609–57618. DOI: 10.1021/acsami.0c17902
4. Eglītis, R., Zukuls, A., Viter, R., Šutka, A. Kinetics of TiO₂ photochromic response in different hole scavenging solvents *Photochemical and Photobiological Sciences*, 2020, 19 (8), pp. 1072–1077

Patents:

1. Latvian patent: P-19-57 Andris Šutka, Anzelms Zukuls, Raivis Eglītis. Method for the enhancement of electrical conductivity of degenerated oxide semiconductors. Accepted 05.04.2022.
2. Latvian patent: P-19-86 Andris Šutka, Kaspars Mālnieks, Raivis Eglītis. Photoactive device for the selective detection of alcohols. Accepted 03.05.2022.

Presentations at conferences:

1. R. Eglītis, A. Šutka, Photochromism of titanium dioxide in various forms. 5th International conference of Applied Surface Science 25.04.2022 – 28.04.2022.
2. R. Eglītis, Photochromic TiO₂/PEGDA organogels. 62nd RTU conference “Materials Science and Applied Chemistry” 22.10.2021.
3. R. Eglītis, A. Šutka, An adaptive smart window device based on the photochromic effect and capable of electricity generation. 61st RTU conference “Materials Science and Applied Chemistry” 23.10.2020.
4. R. Eglītis, A. Šutka, A. Zukuls, Synthesis and photochromic properties of Nb-doped TiO₂ colloidal nanoparticles. 16th Zsigmondy Colloquium “Soft Colloids” 09.03.2020 – 11.03.2020.
5. R. Eglītis, A. Šutka, Photochromic properties of TiO₂. 60th RTU conference “Materials Science and Applied Chemistry” 24.10.2019.
6. R. Eglītis, A. Šutka, A. Zukuls, R. Viter, A Study of the TiO₂ photochromic response kinetics in different solvents. 6th Nano Today conference 16.06.2019 – 19.06.2019.

1. LITERATURE OVERVIEW

In countries that have a weighted average temperature above 15–20 °C, HVAC systems are consuming around a third of all the electricity used in office buildings. Using blinds to block infra-red radiation (heat) increases the usage of artificial lighting, as it also blocks visible light. Alternative to blinds is the usage of tinted films of reflective coatings. A downside of reflective coatings is that there is no option for modulation of optical properties. In cloudy days it is needed to let more daylight into the building. The most advanced option is to use smart windows, which would modulate both visible and infrared light transmittance in response to external stimulus.¹ Currently most of the most widely used smart window technologies are based on electrochromic materials. However, the usage of photochromic and thermochromic materials can be fully autonomous without the need for external power sources.

Photochromic materials, being the second largest family of chromic materials (after electrochromic materials), have slightly overlapping applications with electrochromic materials. The most widely known application for photochromism was and still is self-tinting glasses or eyewear. While first, silver halides were used for these materials initially, they were replaced by organic photochromic compounds dispersed in polycarbonate.² Other applications for photochromic materials are smart windows, light sensitive varnishes, and dyes for clothing, as well as colorimetric UV sensors. Photochromic materials also have been used as optoelectronic materials for data storage³ and as colorimetric oxygen sensors.⁴ For instance, TiO₂, which is a widely known wide band gap semiconductor, can be used normally to achieve positive photochromism. However, when it is combined with methylene blue in an anaerobic matrix, it can achieve negative photochromism, bleaching under UV irradiation.⁴ TiO₂ possesses a combination of different desirable properties: non-toxicity, biocompatibility, as well as optical and electrical properties.⁵ As it is able to absorb UVA light, it has been researched for usage in such fields as photocatalysis⁶, photovoltaics⁷, photoelectrochemistry⁸ as well as photochromics.⁹ The main drawback of anatase TiO₂ is its wide band gap of 3.2 eV and the low quantum yield primarily determined by the fast recombination of the photogenerated charge carriers.¹⁰ This means that to photoexcite the TiO₂, UVA light is necessary. To narrow the band gap, doping can be implemented. Doping is the process of introducing either atoms of different elements (both cations as well as anions) with the same (isovalent doping) or different valence (aliovalent doping). If the dopant has a higher valence, it is called an acceptor dopant that introduces levels near to the conduction band. If, however, the dopant has a lower valence, then it is called a donor dopant and it introduces electron donor levels near to the valence band. Doping also has the effect of distorting the crystalline lattice, as all dopants will have a different size than the host materials ions.

The photochromic properties of titanium dioxide can be observed in several different ways (Fig. 1.1). The easiest is by simply dispersing the nanoparticles in a hole scavenging solvent.¹¹ If this is not possible or desired, another possibility is to prepare heterostructures, either TiO₂-semiconductor or TiO₂-metal¹², as these do not require an additional hole scavenger to be present for photochromism to take place. These can be prepared also in thin film form. Ordinary TiO₂ nanoparticle thin films still need to be immersed in a hole scavenging liquid to undergo photochromism. There are also studies showing that anatase nanocrystals with clearly defined crystalline facets have the possibility of increased charge carrier separation.¹³ This is due to the

fact that electrons and holes tend to migrate to different crystalline facets. Finally, there is also the possibility of preparing gels of TiO₂ nanoparticles in which the nanoparticles are dispersed in a polymer matrix that is also saturated with a hole scavenger. This allows for these composites to act the same way as colloids, but without the drawback of a colloid (evaporation and potential leakage), while also avoiding the problems arising from simple TiO₂ thin films.

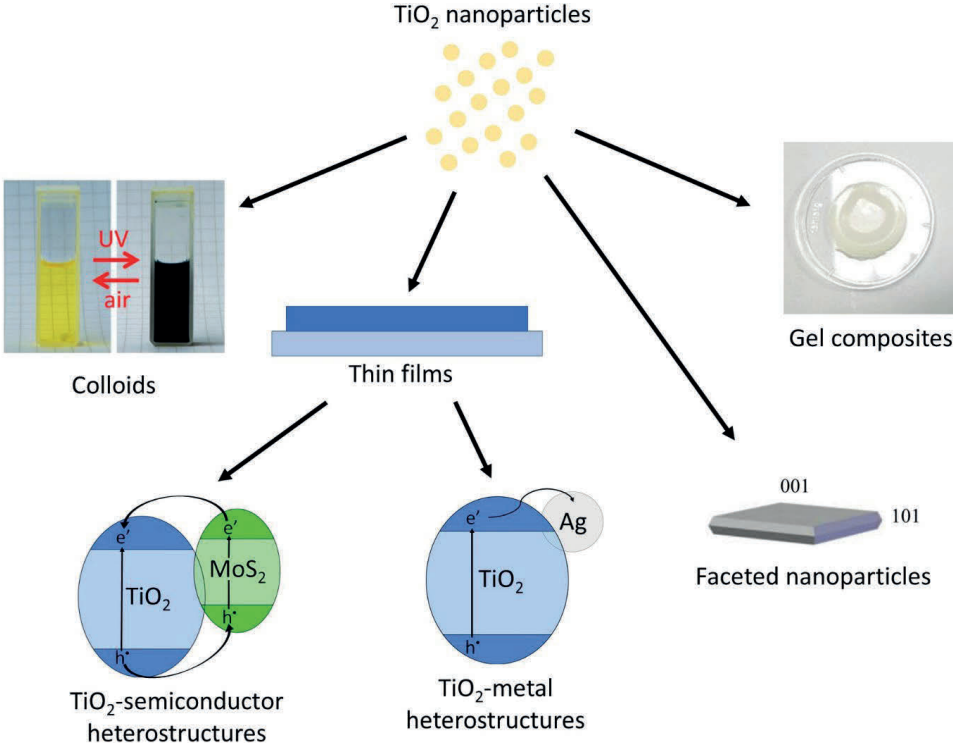
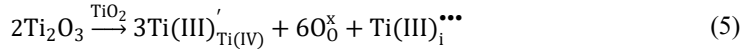
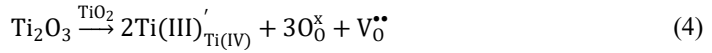
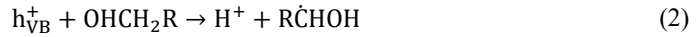


Fig. 1.1. Ways how TiO₂ (and subsequently other TMO) nanoparticles can be implemented for photochromic applications: colloids,¹⁴ thin films, faceted nanocrystals¹⁵ and gel composites.¹⁶

When the material is irradiated with light that has an energy higher than the band gap of the semiconductor, electrons are excited in the valance band. These land in the conduction band, leaving behind a hole (Equation (1)). On the one hand, if this process is happening in an aerobic environment and/or in water, oxygen and water will interact with the electrons and holes respectively, producing ROS. On the other hand, if photoexcitation is happening in an anaerobic environment and in the absence of water, the electrons and the holes are left unaffected and eventually recombine. However, if photoexcitation is done in an anaerobic environment and in the presence of a hole scavenger, such as alcohols,¹⁷ the holes are filled, with the hole scavengers donating electrons to the TiO₂ valence band (Equation (2)). This process results in the oxidation of the hole scavenger¹⁸ and leaves behind an excess of electrons trapped in the conduction band. A part of these electrons will become trapped by reducing Ti⁴⁺ to Ti³⁺ (Equation (3)) in the TiO₂ crystalline lattice. This effectively dopes TiO₂ with Ti₂O₃ and can result in the formation of oxygen vacancies (Equation (4)) or the formation of titanium interstitials (Equation (5)).^{19,20} Because of this, the process is called photodoping.



The defect introduced into the TiO_2 lattice from the photodoping process introduces additional electron donor and acceptor levels in the TiO_2 lattice. Ti^{3+} introduces shallow electron donor levels in the TiO_2 band gap approx. 1.25 eV below the conduction band minimum,²¹ while oxygen vacancies introduce electron acceptor levels in the TiO_2 bandgap between 0.75 eV and 1.18 eV below the conduction band minimum (Fig. 1.2).^{20,22} These levels allow the absorption of visible light by the TiO_2 material, which can be seen as a color change of the material from white to blue. Because of apparent color change when the material is irradiated with light, this is also called photochromism.

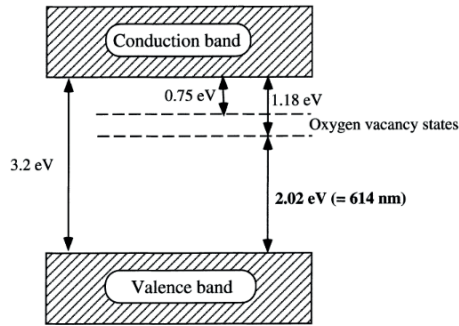


Fig. 1.2. A band structure model for anatase TiO_2 with oxygen vacancies.²⁰

2. METHODS SECTION

2.1. Synthesis of TiO₂ and doped TiO₂ nanoparticles

TiO₂ nanoparticles were synthesized by using a method first described by Scolan and Sanchez.²³ It was further developed by Joost, et al.¹⁴ and was as follows: in a double necked flask under N₂ flow, 12.4 mL of *n*-BuOH (previously dried by adding CaH₂ to it) was added through a syringe and 0.22 μm filter. The necessary amount of AcacH (8.368 mL) was added to the butanol. Then the Ti(*n*BuO)₄ (9.05 mL) was added dropwise. This caused a yellowish solution to form, indicating the formation of a Ti(*n*BuO)_{4-x}(acac)_x complex.²⁴ After this, the solution was brought to reflux and a mixture of 4-DDBSA (1.76 g) and DI water (4.865 g) was added dropwise to the solution. This was then left to react overnight (around 17 hours). After this, the solution was left to cool to room temperature during which a yellow precipitate formed. This was then separated via centrifugation (2000 g, 1 hour) and washed with MeOH. Finally, the purified nanoparticle sediment (white to slightly yellowish) was decanted and redispersed in either pristine *n*-BuOH or DMF, or any other solvent, used in this work (EtOH, *n*-PrOH, *i*-PrOH, *n*-Pentanol or *n*-Hexanol). Subsequently, the nanoparticles can also be covered by a small amount of MeOH and kept in a slurry form for later use. To produce doped TiO₂ nanoparticles, before the addition of 4-DDBSA/DI, the dopant precursor/AcacH solution in *n*-BuOH was added to the synthesis solution. After the 17 h reflux, the solution was cooled to 40 °C and transferred into a 50 mL Teflon lined stainless steel autoclave and solvothermally treated for 24 hours at a temperature of 150 °C. Cooling of the autoclave was done slowly in the oven over the timespan of 6 h. After this, the purification procedure is the same as in the case of un-doped TiO₂ and the nanoparticles are immediately redispersed in pristine *n*-BuOH or DMF.

2.2. Determination of photochromic properties using UV-Vis spectroscopy

The observed kinetic processes had a non-linear nature (Fig. 2.1) and could be classified in different stages (I–IV). During Stage I, any adsorbed water or oxygen is first subjected to photocatalysis. At this stage, the resulting photochromic expression is slow. The coloring speed increases over time. During Stage II, the transmittance change rate can be considered as constant and constitutes the majority of the change in transmittance. In Stage III, the absorption has reached such a degree that the non-linear correlation between absorbance and transmittance results is an apparent slow-down in transmittance change. This is also partly due to saturation of the nanoparticles with photodoping induced defects and photoaccumulated electrons and an equilibrium forming between the formation of new defects and the internal hole scavenging of the newly formed defects. For recovery air is bubbled through the colloid either at a constant speed or a set volume of air was injected and the subsequent change in transmittance was recorded. The colloid goes through the oxidation of the Ti³⁺ and the filling of oxygen vacancies (here aggregated into Stage IV). To compare the kinetics of the change in transmittance of different samples during Stages I–III, the rate was calculated as the 1st order time derivative of the relative transmittance change. This then was examined in terms of the maximum and average transmittance change rates.

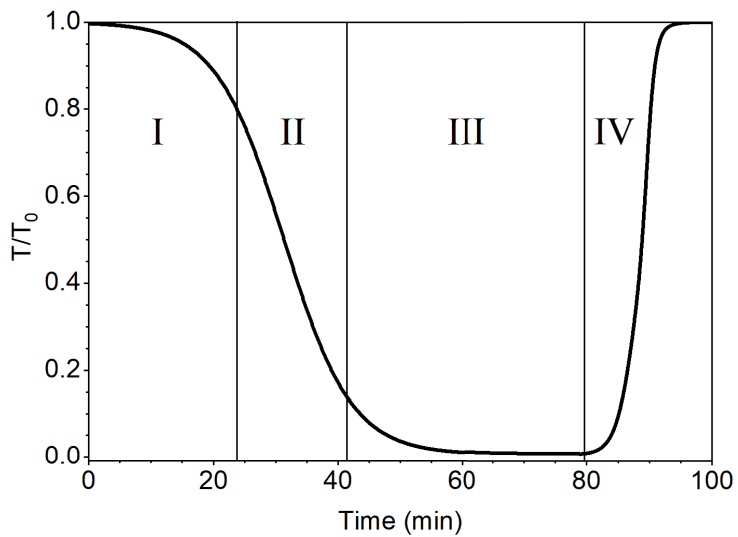


Fig. 2.1. The different stages of photochromism for TiO_2 nanoparticle colloids at 900 nm.

3. RESULTS AND DISCUSSION

3.1. Photochromic properties of titanium dioxide

The synthesized nanoparticles were crystalline according to both TEM and XRD (Fig. 3.1 A, B) with a mean size of 3.6 ± 0.5 nm according to TEM. The nanoparticles comprised the anatase TiO_2 crystalline phase, as indicated by XRD (JCPDS 21-1272) and Raman spectroscopy (Fig. 3.1 C). No amorphous or secondary crystalline phases were detected. The Raman bands visible were located at 148 cm^{-1} (main E_g band), 198 cm^{-1} (secondary E_g band), 398 cm^{-1} (B_{1g} band), 515 cm^{-1} (A_{1g} band), and 638 cm^{-1} (additional E_g band). These values were red-shifted when compared to the values found in literature – 144 cm^{-1} , 197 cm^{-1} , 399 cm^{-1} , 513 cm^{-1} , and 639 cm^{-1} , respectively.²⁵ This is caused by the phonon confinement characteristic of ultrafine nanoparticles.²⁶ The XPS spectra of Ti 2p and O 1s (Fig. 3.1 D, E) indicate a fully oxidized TiO_2 material. The Ti 2p peaks show only Ti^{4+} signals at 464.6 eV and 458.9 eV, while the O 1s spectra shows a O^{2-} signal at 529.7 eV and an additional signal at 531.2 eV usually attributed surface oxygen and hydroxyl groups.²⁷

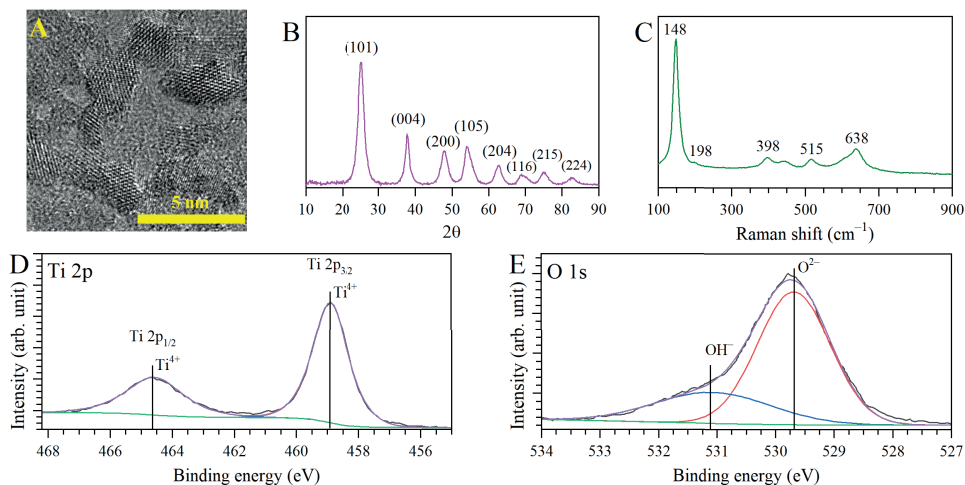


Fig. 3.1. A – TEM micrograph of the TiO_2 nanoparticles; B – XRD diffractogram of the nanoparticles; C – Raman spectra of the nanoparticles; D and E – Ti 2p and O 1s high resolution XPS spectra for the nanoparticles.

The photochromic properties of TiO_2 nanoparticles were studied in different hole scavenger solvents. The main category of hole scavengers studied was different alcohols, as they are capable of easily adsorbing onto the surface of the nanoparticles and partake in the electron donation, i.e., hole scavenging.²⁸ The alcohols studied were ethanol, *n*-propanol, *i*-propanol, *n*-butanol, *n*-pentanol, *n*-hexanol as well as mixtures of ethanol with MEOA, DEOA and TEOA. The nanoparticle concentration was 100 g/L, while the amount of MEOA, DEOA and TEOA was 50 mol% of the amount of TiO_2 present in the colloid. Methanol was not studied because the nanoparticle suspensions in methanol were opaque due to low nanoparticle stability and

agglomeration. All the samples showed photodarkening when the colloids were irradiated with UVA (365 nm) light.

The calculated photodarkening rates for the different solvents are shown in Fig. 3.2. The transmittance change rate at different wavelengths was different. This was because different defects are responsible for photochromism at different wavelength. At 450 nm, the main absorbance stems for the additional intra band gap levels introduced by the oxygen vacancies V_O . At 600 nm the main absorbance comes from the Ti^{3+} defects, bringing acceptor levels near the CB minimum.¹⁴ At higher wavelength (900 nm) the absorbance comes from plasmon resonance due to the photoaccumulated electrons.¹ From the studied colloids it was seen that the highest transmittance change rate was observed at 600 nm with the change rate at 900 nm being quite similar. The high change rate at 600 nm when compared to 450 nm was because, as per defect Equation (4), the formation of one V_O defect is accompanied by two Ti^{3+} defects. The highest transmittance change rate was observed for colloids in ethanol and *n*-butanol with rates of -0.039 min^{-1} , -0.137 min^{-1} and -0.120 min^{-1} for colloids in ethanol and -0.028 min^{-1} , -0.055 min^{-1} and -0.070 min^{-1} for colloids in *n*-butanol at the wavelengths of 450 nm, 600 nm, and 900 nm, respectively. The addition of the ethanolamines to the ethanol colloid caused changes in the transmittance change rates. Out of the three ethanolamines studied only TEOA increased the transmittance change rate at all wavelengths to values of -0.077 min^{-1} , -0.198 min^{-1} and -0.122 min^{-1} at the wavelengths of 450 nm, 600 nm, and 900 nm, respectively. This can be attributed to the higher amount of hydroxyl groups in the TEOA molecule (3 groups per molecule of TEOA) as well as the presence of the nitrogen atom that had an additional electron pair and could scavenge an additional hole.²⁹

The hole scavenger is the most important part for the photodarkening of the samples. The hole scavenging capability is determined by such factors as the redox potential of the hole scavenger²⁹ as well as the adsorption/desorption rates of the hole scavenger and its oxidation products. Another important factor is the stability of the radical species generated via hole scavenging. The main sites for radical generation are the surface Ti^{4+} sites with an adjacent oxygen that allows for adsorption and dissociation of the hydroxyl group of the hole scavenger.²⁸ For fast hole scavenging, the adsorbed scavenger after electron donation should desorb as quickly as possible. As such, photodarkening here could be considered desorption limited. Such photooxidation products (hole scavenging products) as acetone (in the case of *i*-propanol) would remain on the surface longer than acetaldehyde (photooxidation product of ethanol), given that acetone in radical form would be more stable due to its branched structure when compared to the linear structure of the other alcohols studied.³⁰ This would explain the decreased photodarkening rate for colloids in *i*-propanol. Another factor determining the absorption of alcohol molecules on the surface of TiO_2 is the molecular weight of the solvent with lower molecular weight alcohols having a better adsorption coverage.³¹ This, combined with a low photooxidation product stability explains the high photodarkening rate of the colloids in ethanol.

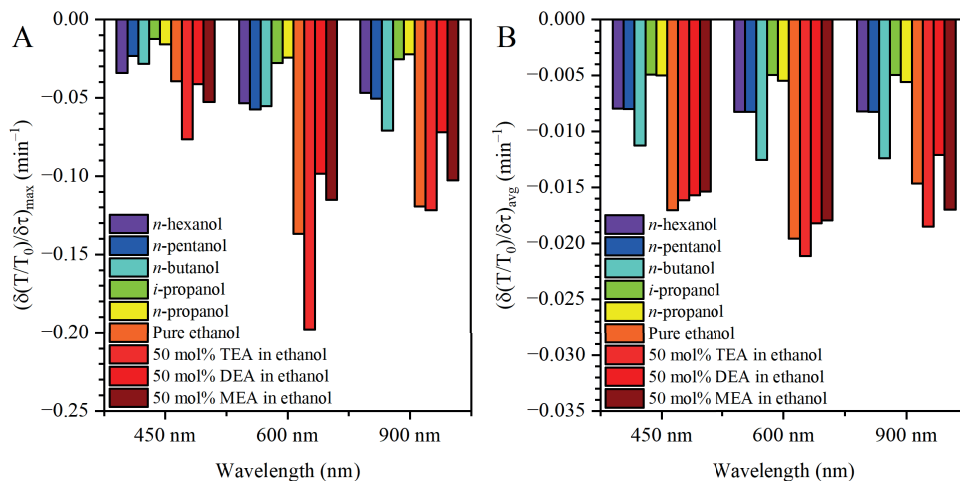


Fig. 3.2. A – maximum transmittance change rate and B – average transmittance change rate for TiO₂ nanoparticle colloids in different hole scavenging media.

The colloids were capable of recovering their initial transmittance when air was bubbled through them. Since the air bubbling speed was kept constant throughout the recovery experiments, the amounts of required air for recovery can easily be converted to recovery rates (Fig. 3.3). The recovery is assumed to be dependent mainly on oxygen solubility. This assumption correlates nearly with all the observed recovery rates, as the oxygen solubility increases in the following sequence – ethanol < *i*-propanol < *n*-propanol < *n*-butanol followed by a slight decrease of *n*-pentanol and *n*-hexanol.³² By comparing the recovery rates at different wavelengths, it can be seen that the annihilation rate of Ti³⁺ defects was higher than compared to V_O or the delocalized electrons. The V_O show the slowest recovery mainly because for each of these defects to be annihilated, two Ti³⁺ defects of delocalized electrons must be quenched. This means that the recovery rate at 600 nm (Ti³⁺ defects) and delocalized electrons (900 nm) should be roughly double of the recovery rate at 450 nm (V_O defects). This is what is also observed with the average recovery rate, for example, for ethanol being 0.004 min⁻¹ at 450 nm and 0.016 min⁻¹ and 0.014 min⁻¹ at 600 nm and 900 nm, respectively. Addition of ethanolamines increases the rate of recovery several times, with TEOA increasing both the maximum and average recovery rates 6 and 7.2 times, respectively. The increase in recovery stemming from the addition of ethanolamines can be attributed to the fact that amino groups can be oxidized to nitro groups, which can function as electrons scavengers.³³

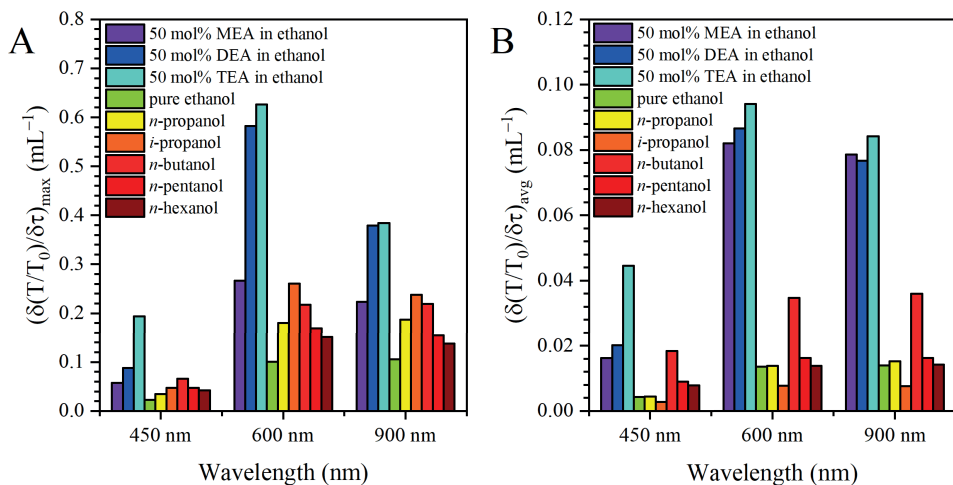


Fig. 3.3. A – maximum recovery rate and B – average recovery rate for TiO₂ nanoparticle colloids in different hole scavenging media.

The photodarkening was accompanied by electron accumulation. This was responsible for absorption in the NIR wavelength range. These photoaccumulated electrons can be scavenged by Fe(acac)₃. This can be used to determine the amount of these electrons via spectrometric titration with a Fe(acac)₃ solution. These photoaccumulated electron values are similar, showing that this property of photodoping is inherent to the nanoparticles themselves, with only a slight influence stemming from the hole scavenging medium, with the electron concentration increasing from 2.01×10^{20} – 2.60×10^{20} cm⁻³ in the row *n*-propanol < ethanol < *n*-hexanol < *n*-pentanol < *i*-propanol < *n*-butanol (Table 1). These values are similar to values previously reported in literature³⁴ and are similar to the values reported for other doped TiO₂ samples, such as carbon doped TiO₂.³⁵ This shows that photodoping can be used to modify the amount of charge carriers in the material similarly to conventional doping.

Table 1

Electron Concentration for Colloids in Different Solvents	
Solvent	Electron carrier concentration (cm ⁻³)
Ethanol	$(2.10 \pm 0.168) \times 10^{20}$
<i>n</i> -propanol	$(2.01 \pm 0.168) \times 10^{20}$
<i>i</i> -propanol	$(2.52 \pm 0.168) \times 10^{20}$
<i>n</i> -butanol	$(2.60 \pm 0.168) \times 10^{20}$
<i>n</i> -pentanol	$(2.26 \pm 0.168) \times 10^{20}$
<i>n</i> -hexanol	$(2.18 \pm 0.168) \times 10^{20}$

The type of point defect formed in TiO₂ during UV irradiation was determined using EPR spectroscopy. The EPR spectra were taken for TiO₂ colloid in *n*-BuOH. Prior to UV irradiation, the un-doped TiO₂ nanoparticles exhibited three EPR peaks at *g*-values of 2.0238, 2.0098 and 2.0036 (Fig. 3.4 A). These are attributable to the signal coming from Ti⁴⁺ and O²⁻.³⁶ During UV irradiation these three signals are replaced by a new and much more intense signal at a *g*-value

of 1.957 with a line width $\Delta H = 12.9$ G. This signal is attributed to Ti^{3+} .³⁷ This signal increased in intensity with irradiation time, reaching a maximum after 60 min of irradiation (Fig. 3.8 B). The amount of Ti^{3+} corresponding to this signal was calculated with the help of an internal standard (Bruker ER 4119HS-2100) with a known spin concentration. The maximum Ti^{3+} concentration was determined to be 3.01×10^{-3} % or 1.812×10^{21} spins/mol after 60 min irradiation. This shows that the main defect in the photodoped TiO_2 is Ti^{3+} . However, similarly to what has been shown before, the vast majority of the photoaccumulated electrons populate the conduction band, and only a small amount (0.34 %) of these electrons have taken part in the formation of Ti^{3+} .

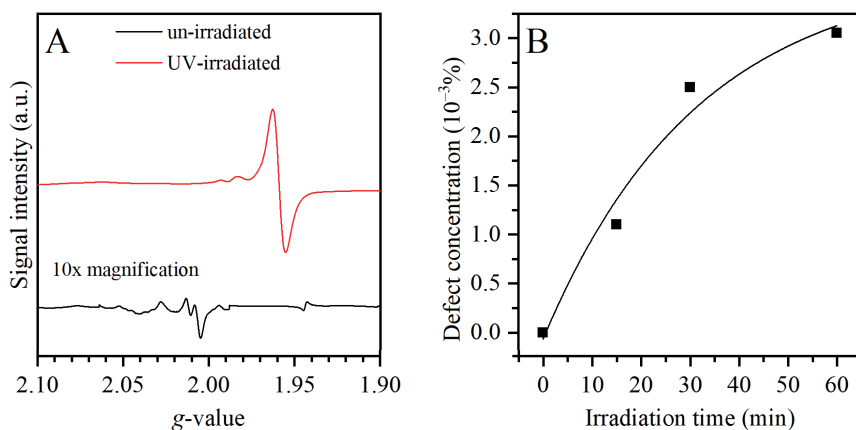


Fig. 3.4. A – EPR spectra for the un-doped TiO_2 nanoparticle colloid at different UV irradiation times; B – Ti^{3+} defect concentrations as a function of irradiation time.

3.2. The electrical properties of titanium dioxide thin films under UV illumination and in the presence of hole scavenger vapors

As the TiO_2 nanoparticles were capable of accumulating electrons in the conduction band when undergoing photodoping, this would imply that there would be a change in their electrical resistance under photodoping conditions. To measure the resistance of the nanoparticles, thin films of TiO_2 nanoparticles were prepared via spin-coating on ITO electrodes. This sample, when irradiated with UV light (365 nm), exhibited a slight decrease in its resistance from the original $1.5 \times 10^9 \Omega$ to $1.1 \times 10^9 \Omega$. This resulted in a change in response of $S = 1.36$ (Fig. 3.5 A). This slight decrease in resistance can be attributed to the photoconductivity of the TiO_2 upon UV illumination.³⁸ The opposite reaction was observed when the sample was exposed to ethanol vapor at a concentration of 1000 ppm in the dark. This resulted in an increase in the resistance of the sample from $1.5 \times 10^9 \Omega$ to $1.17 \times 10^{10} \Omega$ with a response of $S = 7.8$ (Fig. 3.5 B). This increase can be attributed to the ethanol absorption on the sample film.³⁹ The absorption increased the barrier height between the nanoparticles, which in turn decreased the change of electron tunneling between the adjacent nanoparticles.⁴⁰ When the sample was exposed to ethanol vapor and under UV irradiation, the response was the complete opposite to the response in the dark. The sample's resistance dropped from the initial $1.1 \times 10^9 \Omega$ all the way to $7.8 \times 10^6 \Omega$, resulting in a response of $S = 141$ (Fig. 3.5C).

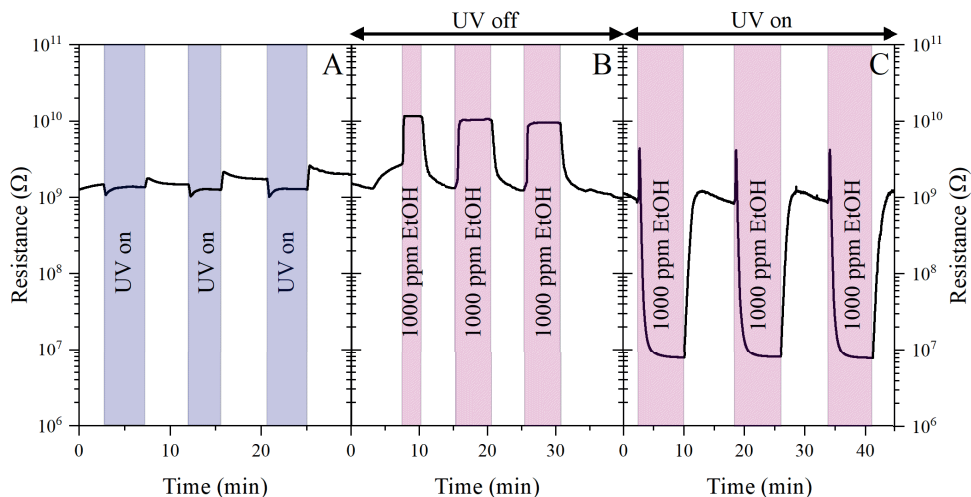


Fig. 3.5. A – change in resistance when switching UV light on and off without solvent gas at a flux density of 46 mW/cm²; B – change in resistance when adding EtOH (1000 ppm) and ventilating the chamber without UV light; C – change in resistance when adding EtOH (1000 ppm) and ventilating the chamber while irradiating with UV light.

The dramatic decrease in resistance under UV and 1000 ppm EtOH can be attributed to the hole scavenging nature of ethanol seen when the nanoparticles were dispersed in the solvent. As the electron-hole pairs are generated under UV light, ethanol, which adsorbs on the surface of the nanoparticle thin film, scavenges the holes leaving behind the electrons. When the test chamber was vented and the ethanol vapors were removed from the air in the chamber, the oxygen present in the air scavenged the accumulated electrons, allowing the samples electrical resistance to return to its original value. The oxygen requirement was confirmed by repeating the experiment in a purely N₂ atmosphere (Fig. 3.6 A). After the drop in resistance caused by the introduction of EtOH vapor, when the chamber was flushed again with N₂, the resistance no longer returned to its initial value. During the next 100 min the resistivity increased only slightly, possibly due to thermal relaxation (in comparison with oxygen the resistance recovered within 3 min). This phenomenon has been observed previously and has been termed persistent photoconductivity.⁴¹ This shows that oxygen can also be used to measure the amount of photoaccumulated charge carriers.

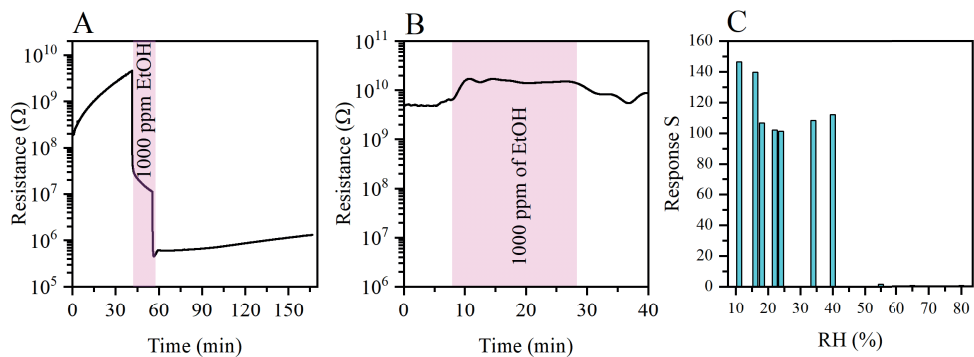


Fig. 3.6. A – resistance change when the samples resistance was measured in a N_2 atmosphere while irradiating with a UV LED with a light intensity of 46 mW/cm^2 ; B – the resistance changes of the sample during irradiation with a 10W commercial visible LED light when adding EtOH to the chamber; C – the response S of the sample at different relative humidity when irradiating with a UV LED with a light intensity of 33 mW/cm^2 and exposed to 1000 ppm EtOH.

To evaluate whether the TiO_2 nanoparticles thin film sample changes its resistance only under UV light irradiation, an experiment was conducted by swapping the UV LED array with a 10W commercial white LED light with a wavelength range of 410–750 nm. When the sensor sample was exposed to the same ethanol vapor concentration as before (1000 ppm), only a marginal increase in the resistance of the sample was seen (Fig. 3.6 B), similar to that seen when the sensor was exposed to ethanol vapor in the dark. This acts as a confirmation of the theory that for electron accumulation, UV light is necessary. When looking at the samples charge accumulation abilities in different humidity (Fig. 3.6 C), it can be observed that there are limitations to the environments in which this sample can accumulate electrons. At low RH of 10–16 %, the change in resistance is the highest, reaching a response of 140–146. This is mainly due to the fact that such low RH values consequently cause part of the adsorbed water molecules to desorb from the surface for equilibrium with the surrounding air, exposing more of the hole scavenging sites, thus increasing the change in transmittance. The response drops to 101–112 when exposed to RH of 18–40 %. These RH values are a lot more common in the ambient environment, especially in countries with a milder climate, showing that photoelectrons can accumulate in an ambient environment. However, above $RH = 40 \%$, the change in resistance drops to just 1.6 and lower when exposed to the same amount of EtOH and UV. This could be attributed to the formation of a mono-layer of liquid water on the surface of the sample thin film. As this layer is more conductive than the semiconductor material itself, it would then provide a charge screening effect and electric conductivity via Grotthuss proton jumping.⁴²

The samples response to ethanol vapor was dependent on the concentration of the vapor and could also be varied by modulating the UV light intensity (Fig. 3.7 A). This indicates that substantial amounts of ethanol vapor are necessary to saturate the sample with photoaccumulated electrons. As the change in resistance is UV light intensity dependent, this would mean that the hole scavenging rate could be considered the limiting step of the

photoaccumulation process. At a low irradiation intensity (15 mW/cm²) the response, i.e., the change in resistance (response) increased from 1.6–75 in a linear manner when the ethanol vapor concentration was varied from 100–1000 ppm. When the ethanol vapor concentration was decreased to just 50 ppm, no noticeable change in resistance was observed, indicating an insufficient amount of photoelectron accumulation. When the UV light intensity was increased to 33 mW/cm², the response also increased from 2.8 to 138 in the ethanol vapor range of 100–1000 ppm. Furthermore, at this light intensity the sample also exhibited a very low response (1.34) to 50 ppm of ethanol vapor. This indicated that at such a light intensity enough photoelectrons are excited for hole scavenging to happen and hence photoaccumulation and resistance change. A further increase in the UV light intensity to 47 mW/cm² resulted in further increase in response to 37 at an ethanol vapor concentration of 100 ppm to 170 when the ethanol concentration increased to 1000 ppm. Also, at this light intensity, the sample showed a response of 18.4 to ethanol vapor at 50 ppm ethanol and 18 at an ethanol vapor concentration of just 25 ppm. It can be observed that at this UV light intensity the response is no longer linear but shows that saturation starts to occur. This is due to the fact that the hole scavenging rate with ethanol absorption becomes the rate limiting factors.

The TiO₂ thin film sample exhibited a resistance change response to not only ethanol vapor but also hole scavengers in general. When exposing the sample to different solvent vapors – both polar and non-polar – solvents (Fig. 3.7 B) the photoinduced electron accumulation was different. The change in resistance due to photoaccumulated charge carriers was similar as it was when the TiO₂ nanoparticles were dispersed in the corresponding hole scavenger solvent. These results also confirm that to successfully scavenge the photogenerated holes, the analyte gas molecules should contain hydroxyl groups, as these can adsorb onto the TiO₂ surface.²⁸ The low affinity towards acetone can be explained by the fact that aldehydes can also function as hole scavengers, but very mild ones. Furthermore, acetone has a tautomeric enol form, which has a hydroxyl group and is present in very small quantities in acetone.³⁰ As toluene and *n*-hexane lacks this groups, then this pathway is not available for these solvents. The resistance change response to alcohol falls in order *n*-butanol > *n*-hexanol > *n*-propanol > methanol > ethanol > *i*-propanol > *n*-pentanol > acetone. *N*-butanol is known for its effective photogenerated hole scavenging properties from TiO₂.¹⁴ It has been shown that the hole scavenging process on the surface results in alkoxy radicals.³⁰ The alkoxy radical stability increases with an increase in the branching and size in the carbon backbone.³⁰ A secondary alcohol, such as *i*-propanol and heavier alcohols, such as *n*-pentanol and *n*-hexanol, produce more stable radicals. The photogenerated holes oxidize alcohols to aldehydes and in the case of *i*-propanol and acetone are stable on the TiO₂ surface at 300 K.⁴³ The stable adsorbates do not desorb and limit adsorption of additional hole scavenging alcohols, resulting in a lower photoaccumulated electron concentration. Furthermore, depending on the complexity of the alcohol, the reaction rate varies, resulting in a varied resistance response of the material.

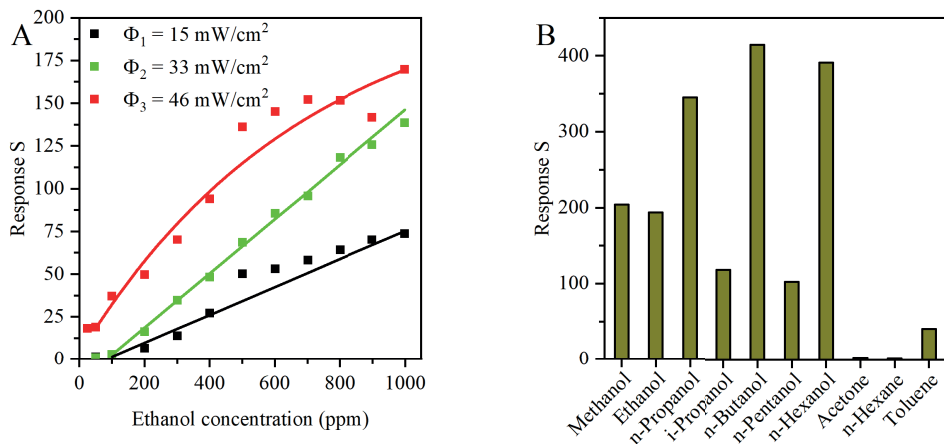


Fig. 3.7. A – response S while changing the EtOH vapor concentration and while irradiating the sensor with different intensity UV light; B – response S when exposing the sample to different solvents at a concentration of 1000 ppm and while irradiating the sample with UV light at an intensity of 47 mW/cm^2 .

3.3. Photoelectron accumulation in titanium dioxide films under UV irradiation while submersed in a hole scavenger

Since the TiO_2 nanoparticles exhibited electron accumulation in thin film form when exposed to hole scavenger vapor, the next possibility would be to see how the thin film exhibits photoelectron accumulation when immersed in a hole scavenger. This was realized by using a thicker TiO_2 thin film with a thickness of 1075 nm (Fig. 3.8 A) that was immersed in *n*-butanol. Current generation was looked at in order to evaluate the amount of photoaccumulated electrons between the thin film and a counter electrode at different supplementary resistances. A Pt wire was used as a counter electrode. The sample could generate $1.35 \mu\text{A}$ of continuous current and $2.6 \mu\text{A}$ of peak current (Fig. 3.8 B, C). The continuous current was reduced when resistance was added to the circuit, while the potential increased inversely proportional to the current reaching a maximum of 398 mV. This was because adding resistance decreased the number of electrons flowing through the external circuit, thus allowing for a larger potential difference to build up. The maximum power generated from the sample was $0.023 \mu\text{W/cm}^2$. This has the potential of being used to power different low-power consumption sensors as an alternative to solar cells.

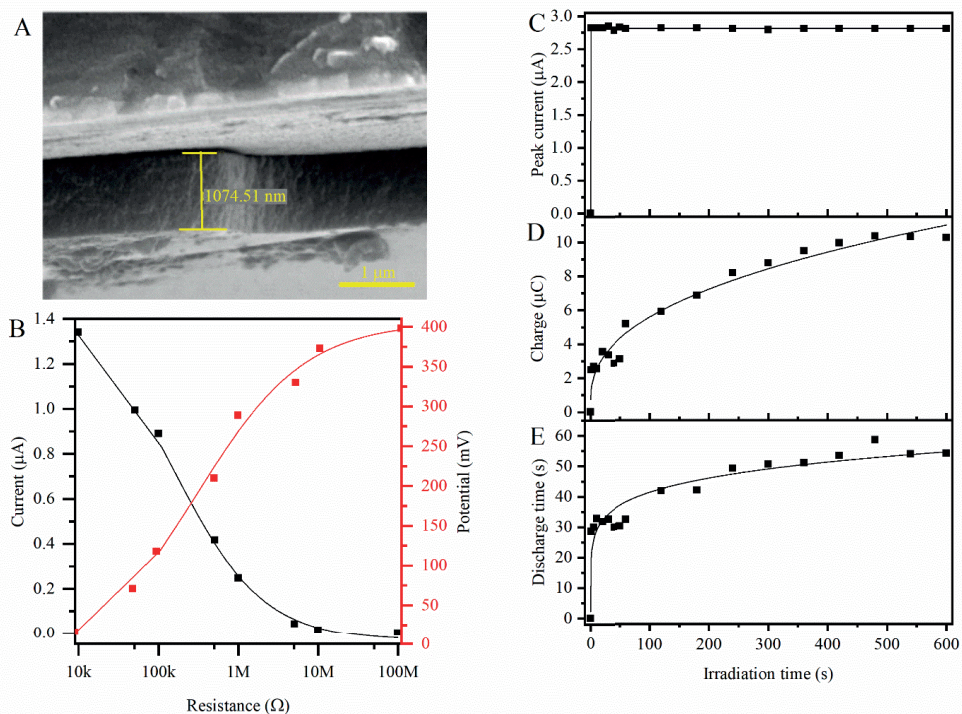


Fig. 3.8. A – SEM micrographs of the used thin film; B – current and potential graphs for continuous measurements; C–E – electric properties of the film as a function of irradiation (charging) time.

Under open circuit conditions a charge could be built up on the thin film in the form of photoexcited electrons, which accumulated in the conduction band of the TiO_2 , with no noticeable change in color. While the peak current that could be reached was independent from irradiation time (reaching the maximum after just 1 second), the discharge time and subsequently the accumulated charge gradually increased, reaching saturation after 5 minutes of irradiation. This showed that with an irradiation time of 5 min it was possible to saturate the sample with photoaccumulated electrons. The maximum amount of charge that was scavenged this way from the sample was just $10.2 \mu\text{C}$ that corresponds to approx. 6.4×10^{13} electrons of the sample. When converted to charge carrier concentration, this equates to an electron concentration of $1.17 \times 10^{17} \text{ cm}^{-3}$, which is several orders of magnitude lower than it was obtained from the spectrometric titration results ($2.6 \times 10^{20} \text{ cm}^{-3}$). This could be because in thin film form the lower layers of the film do not really interact with the hole scavenger, meaning that the upper layer of the thin film experiences electron photoaccumulation. Nevertheless, these results also show that the photoaccumulated charge carrier concentration can also be studied using charging when immersed in a hole scavenger not only when exposed to its vapors.

3.4. The influence of Nb⁵⁺ dopant on photochromic response of titanium dioxide

Niobium Nb⁵⁺ was chosen as the dopant because of its small size difference with regards to Ti⁴⁺ (Nb⁵⁺ (78 pm) and Ti⁴⁺ (75 pm)) as well as its electron acceptor nature. The other candidates such as V⁵⁺ or Ta⁵⁺ were found to either cause persistent visible light absorption or a reduced photochromic effect. The Nb⁵⁺ dopant content was varied from 1 to 20 at%. As seen from the Raman, XRD and SAED results, all the nanoparticles synthesized with a nominal Nb⁵⁺ content from 1 at% to 20 at% were composed solely of anatase (JCPDS 21-1272).⁴⁴ This shows that doping with Nb⁵⁺ did not promote the creation of any secondary phases. Doping with Nb⁵⁺ caused the shift of the 152 cm⁻¹, 402 cm⁻¹ and 642 cm⁻¹ bands from 152 cm⁻¹ to 150 cm⁻¹, 402 cm⁻¹ to 388 cm⁻¹ and 642 cm⁻¹ to 639 cm⁻¹, respectively (Fig. 3.9). The 152 cm⁻¹ band also increased in width due to the formation of Nb-O-Ti bonds⁴⁵ and deformation of the Ti sublattice and the stretching of the Ti-O bonds.²⁶ The 642 cm⁻¹ also increased in intensity and red-shifted due to the formation of Nb-O bonds. The shift of the B_{1g} mode peak at 402 cm⁻¹ with increasing Nb⁵⁺ content is another confirmation of successful Nb⁵⁺ incorporation in the TiO₂ crystalline lattice, as this mode stems from the Ti-O bond stretching.⁴⁶

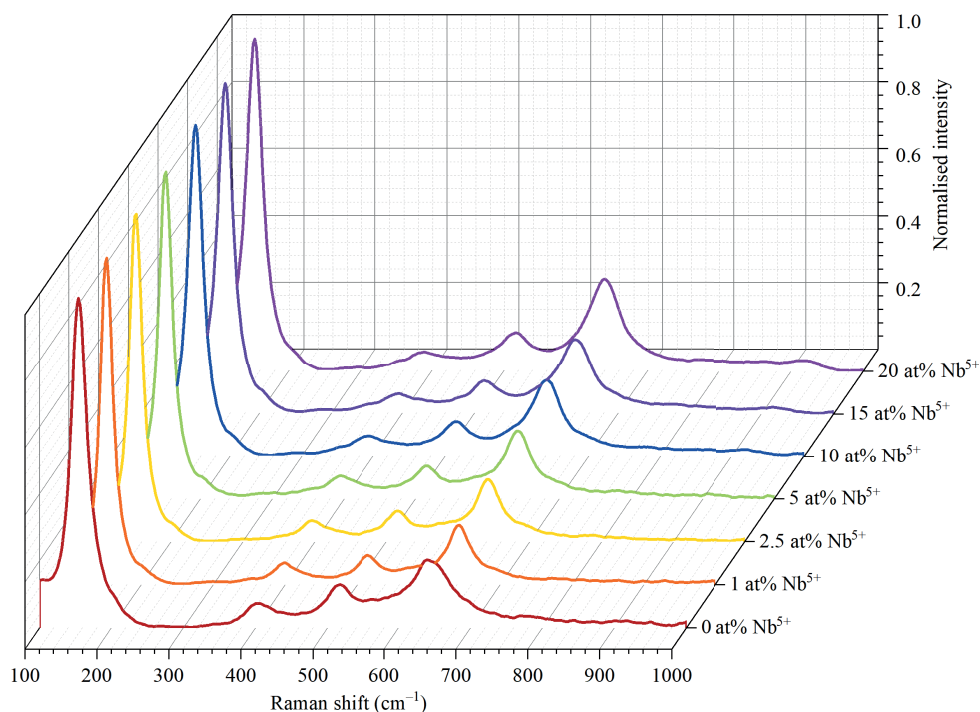


Fig. 3.9. Raman spectroscopy results for un-doped and Nb⁵⁺ doped TiO₂ nanoparticles.

The XRD results (Fig. 3.10) showed diffraction peak shifts with increasing Nb⁵⁺ dopant. The main anatase peak of (101) showed a shift of 2θ values from 25.305 to 25.188, which is indicative of increased lattice spacing.²⁶ This is an indication that Ti⁴⁺ cations with a size of 75 pm were substituted with slightly larger Nb⁵⁺ cations with a size of 78 pm.⁴⁷ Another

observation is the shift of some higher index plane peaks, such as (211) and (220). This stems from the increase in lattice spacing that corresponds to the index planes in question. The Rietveld refinement results showed that doping with the larger Nb^{5+} cations caused an increase in both crystalline lattice parameters from $3.791 \pm 0.001 \text{ \AA}$ to $3.807 \pm 0.001 \text{ \AA}$ for parameter a and from $9.506 \pm 0.002 \text{ \AA}$ to $9.554 \pm 0.001 \text{ \AA}$ for parameter c , respectively, when comparing the un-doped TiO_2 NCs and the sample with a 20 % Nb^{5+} content. Subsequently, the unit cell volume increased from 136.618 \AA^3 to 138.493 \AA^3 .

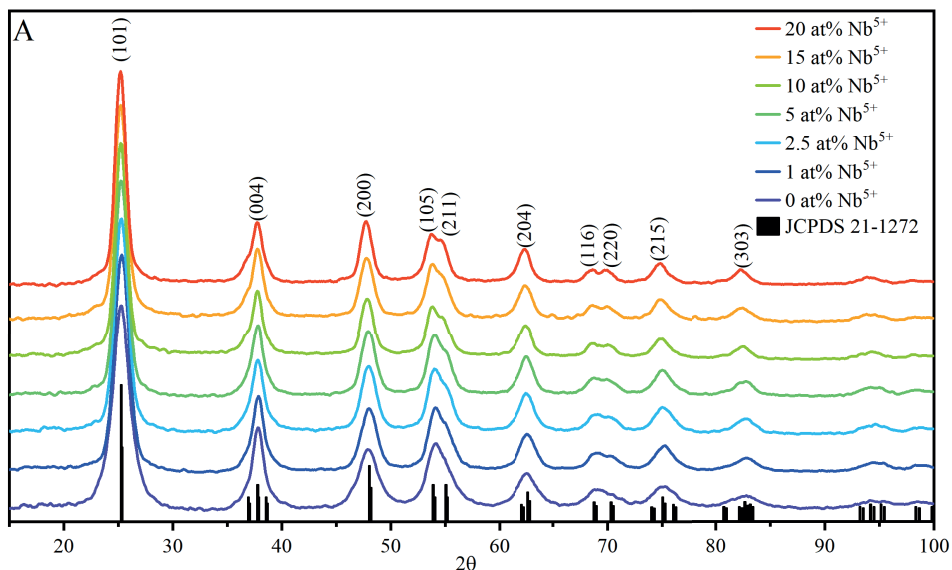


Fig. 3.10. XRD of the samples with different Nb^{5+} content

The TEM micrographs (Fig. 3.11 A–G) showed that the nanoparticles were monocrystalline and without any signs of either being amorphous or having a core-shell structure. The nanoparticles were uniformly sized, with no large agglomerates present. Another conformation of the crystalline nature of the nanoparticles stems from the SAED diffractograms (see Fig. 3.11 H–I). The coaxial ring patterns are indicative of polycrystalline samples. This is because the electron beam hits a multitude of nanoparticles, showing polycrystalline diffraction rings instead of discrete monocrystalline diffraction patterns. The rings themselves corresponded to the same diffraction peaks from XRD diffractograms and corresponded to the (101), (004), (200), (105), (204), (220) and (215) planes.⁴⁸ From the TEM micrographs, 100 measurements of the nanoparticle sizes were taken using ImageJ software. These measurements were then used to calculate the mean $d(50)$ size of the nanoparticles as a function of Nb^{5+} content. The nanoparticle size increases logarithmically from $3.6 \pm 0.5 \text{ nm}$ for the un-doped samples to $6.7 \pm 1.0 \text{ nm}$ for the samples with a Nb^{5+} content of 20 at%.

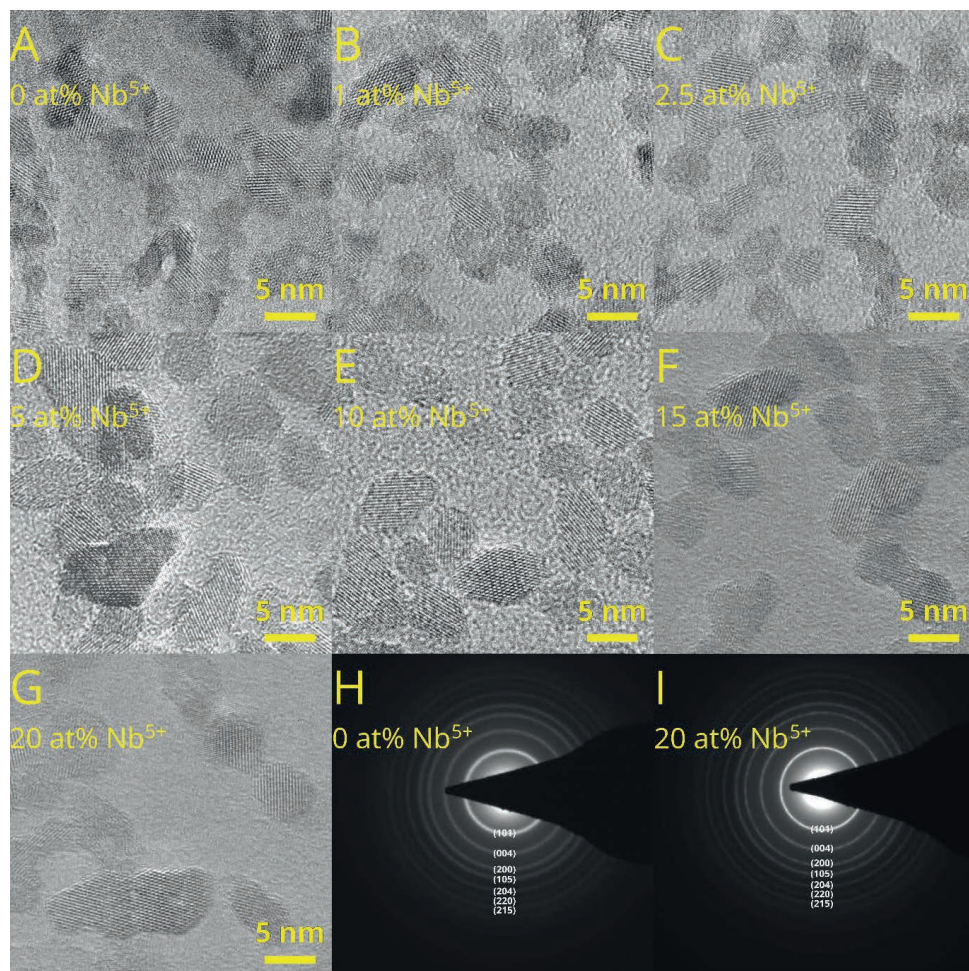


Fig. 3.11. A–G – high resolution TEM images of the synthesized nanoparticles with different Nb content; H and I – selected area electron diffraction pattern for pure TiO₂ and TiO₂ with 20 % Nb.

The overview of XPS spectra of all the doped TiO₂ samples (Fig. 3.12 A) showed the presence of O, Ti and Nb with no additional stray elements present. The 3d and C 1s signals stem from the sample holder and organic contamination, respectively. The binding energy of the Ti 2p 3/2 peak at 458.5 eV and 2p 1/2 peak at 464.2 eV indicates fully oxidized TiO₂, with a homogeneous Ti⁴⁺ oxidation state (Figure 3.12 D), while the Nb 3d peaks at slightly above 207 eV and 209.9 eV indicate fully oxidized Nb⁵⁺ with no indication of other Nb oxidation states (Fig. 3.12 C). The O 1s peak consists of two overlapping peaks at 530 eV and 531 eV (Fig. 3.12 B). The main peak at 530 eV corresponds to lattice oxygen in the bulk oxide. The broad and weak peak at 531 eV is usually attributed to surface hydroxide groups. According to this data it was determined that the samples in their un-irradiated state do not contain any Ti³⁺ or V_O. This is contrary to other authors.⁴⁹ The difference can be attributed to the different synthesis methods used. As the doped nanoparticles are synthesized using a solvothermal treatment, the increased pressure could retard V_O formation. Using the ratio of Ti 2p and Nb 3d

peaks, the Nb⁵⁺ content was calculated as a function of nominal dopant content (Fig. 3.12 E). These calculated values were in good agreement with the theoretical Nb⁵⁺ content, resulting in a very high doping efficiency (99–100 %). This can be attributed to the minor size difference between both cations of Ti and Nb.

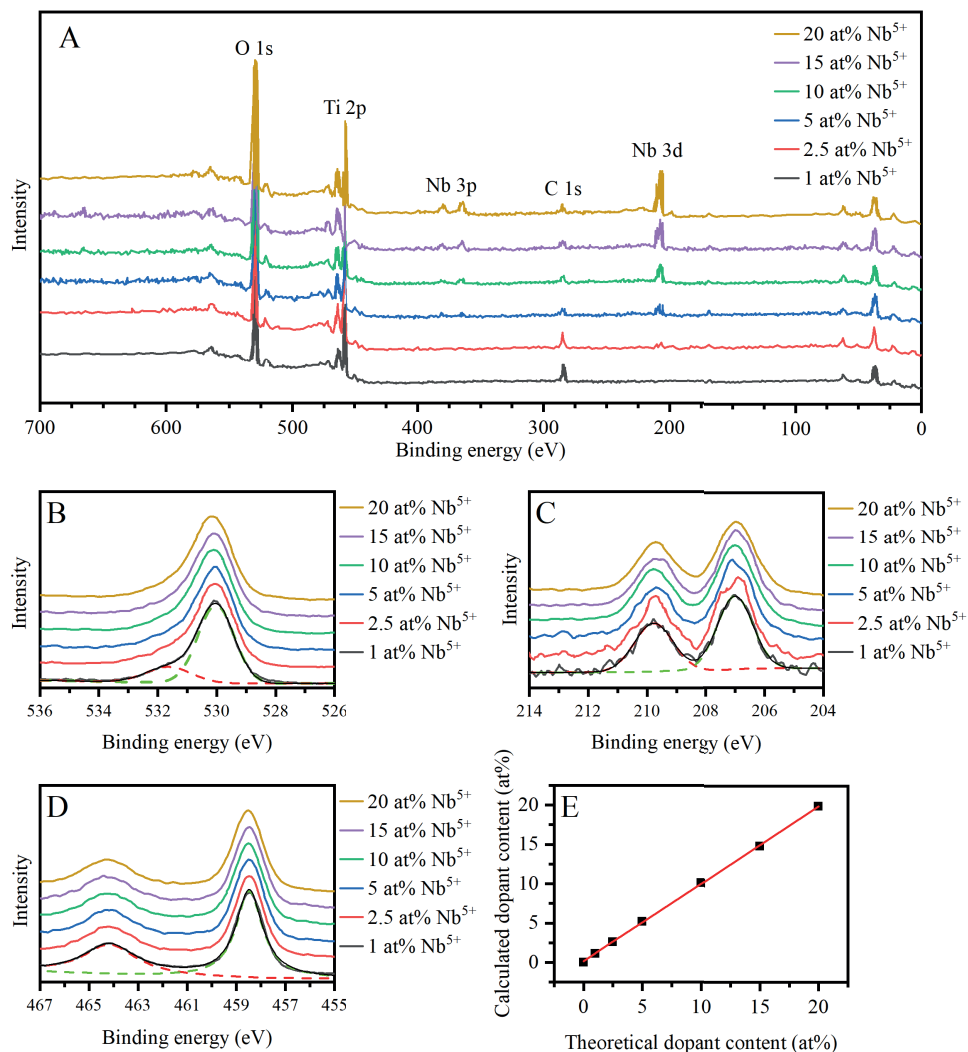


Fig. 3.6. A – overview of XPS spectra of the Nb⁵⁺ doped TiO₂ samples; B, C, D – high-resolution XPS spectra of O 1s, Nb 3d and Ti 2p binding energy regions, respectively; E – calculated dopant content vs theoretical dopant content.

The colloids show a more rapid change in transmittance, which was shown previously in Subchapter 3.1. This is because there the UVA light source had a higher power output of 47 mW/cm² compared to the 25 mW/cm² used in the previous photochromic experiments. Doping with Nb⁵⁺ caused a dramatic decrease in the ramp up time with transmittance already starting to decrease after the 1st minute (Fig. 3.13.). This could be explained by lower

recombination rate of photogenerated charge carriers, which led to the intensified ox-red processes on surface.

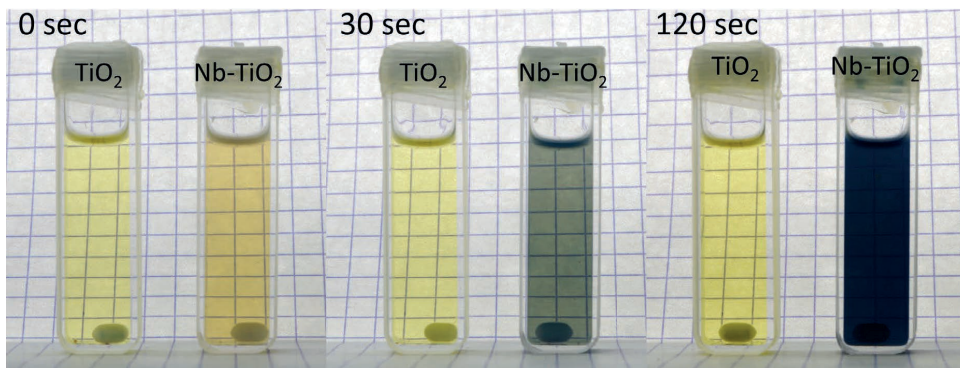


Fig. 3.13. Photographs of undoped TiO₂ and Nb-doped TiO₂ (20 at%) colloids in *n*-butanol, irradiated 0, 30 and 120 seconds showing the strong increase in the photodarkening rate caused by Nb-doping.

To determine the influence of Nb⁵⁺doping on total transmittance change of the TiO₂ nanoparticles in the infrared and visible range, the colloids were diluted to a smaller nanoparticle concentration (2 g/L). Before irradiation, the Nb⁵⁺ doped TiO₂ nanoparticle colloids did not exhibit decreases in transmittance when compared to the un-doped TiO₂ colloid. The photodarkened state of these colloids with a nanoparticle Nb⁵⁺ dopant content of 1–5 at% had a slight decrease in the absorption between 400–550 nm, while in the NIR range (700–1100 nm) the colloids showed higher absorption (Fig. 3.14). Higher Nb⁵⁺ doping resulted in a decrease also in the transmittance at shorter wavelengths of 400–550 nm. The added absorption intensity due to Nb⁵⁺ doping led to total blocking (<2 % transmittance) in the NIR range for samples of 700–1100 nm when the Nb⁵⁺ content was high (10–20 at%). This showed that even at this dilution the nanoparticle colloids were capable of total light blocking in the NIR wavelength range. This also was evident when looking at the absolute transmittance change (Fig. 3.14.) the un-doped TiO₂ colloids had an absolute transmittance change ranging from only 30 % at 400 nm to 76 % at 800–1100 nm. Samples with a low Nb⁵⁺ dopant content (1–5 at%) had an absolute transmittance change that was slightly lower than the un-doped TiO₂ colloid in the visible wavelength range while having a higher transmittance change in the NIR wavelength range with values between 24 % at 400 nm to 98 % at 1000 nm. The samples with higher Nb⁵⁺ dopant content (10–20 at%) had a higher absolute transmittance change in both visible and NIR ranging from 38 % at 400 nm to 99 % at 1000 nm and reached full saturation at this dilution.

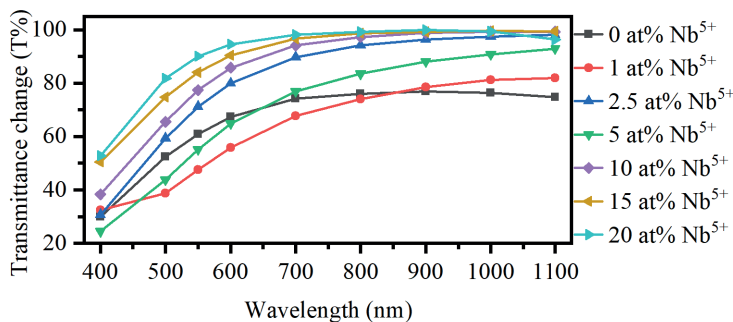


Fig. 3.7. Absolute transmittance change for samples with different Nb-content.

Doping with Nb⁵⁺ resulted in an increase in the absorption within the NIR range because of the increase in the amount of photoaccumulated electrons. This was evident also when determining the accumulated charge carrier concentration. The calculated values ranged from $1.74 \times 10^{20} \text{ cm}^{-3}$ to $4.03 \times 10^{20} \text{ cm}^{-3}$ with the Nb⁵⁺ content increasing from 0 at% to 20 at% (Table 2). Charge carrier concentrations of this magnitude have previously been reported for nanoparticles when they have been doped electrochemically.⁵⁰

Table 2

Photoaccumulated Electron Concentration of the Samples with Different Nb⁵⁺ Content

Nb ⁵⁺ content (at%)	Photoaccumulated electron concentration (cm ⁻³)
0	$(1.74 \pm 0.168) \times 10^{20}$
1	$(1.94 \pm 0.168) \times 10^{20}$
2.5	$(2.11 \pm 0.168) \times 10^{20}$
5	$(2.53 \pm 0.168) \times 10^{20}$
10	$(3.32 \pm 0.168) \times 10^{20}$
15	$(3.80 \pm 0.168) \times 10^{20}$
20	$(4.03 \pm 0.168) \times 10^{20}$

Nb⁵⁺ doping has a profound influence on the photodarkening properties of TiO₂ nanoparticles not only in terms of photodarkening speed but also the absorption intensity. The reason for this is that Nb⁵⁺ introduces excess positive charge that increases electron accumulation as well as the secondary defects introduced into the anatase TiO₂ crystalline lattice to compensate the electrical charge imbalance caused by substituting Ti⁴⁺ with Nb⁵⁺, such as e', V_{Ti}^{'''} or O_i[']. During photodarkening of un-doped TiO₂, all the electrons, which are localized, reduce Ti⁴⁺ to Ti³⁺ and in this way generate V_O^{••}. When Nb⁵⁺ is present in the TiO₂ lattice, it is favored by the excited electrons and reduces Nb⁵⁺ to Nb⁴⁺. This also causes the secondary defects to change to preserve charge neutrality. The photodarkening rate (Fig. 3.15 C, F) increased with the increase in Nb⁵⁺ content, reaching a value of -1 min^{-1} for the sample with a Nb⁵⁺ content of 20 at% at 1000 nm.

It was seen that during recovery there was a gradual decrease in the achieved recovery with increasing Nb⁵⁺ content. Samples that had a Nb⁵⁺ content of 5 at% and higher required more than 20.0 mL of air, which was 6.7 times the volume of the colloid. The samples with 20 at%

Nb^{5+} recovered to only 17 % at 500 nm and recovered 0–3 % in the whole NIR range, indicating that they still possessed many accumulated electrons. The transmittance change rate of the dynamic recovery (Fig. 3.15 D, G) was the highest recovery rate for the un-doped TiO_2 colloid, reaching a maximum change rate up to 0.502 mL^{-1} and average up to $9.46 \times 10^{-2} \text{ mL}^{-1}$ at the NIR wavelength range with the recovery rate highly dependent on the wavelength in the visible range. These values dropped gradually with increasing Nb^{5+} doping content and dropped by more than an order of magnitude in the NIR range for both maximum and average recovery rate, to $1.38 \times 10^{-3} \text{ mL}^{-1}$ and $2.65 \times 10^{-4} \text{ mL}^{-1}$ at 1000 nm, respectively when the nanoparticle Nb^{5+} dopant content reached 20 at%.

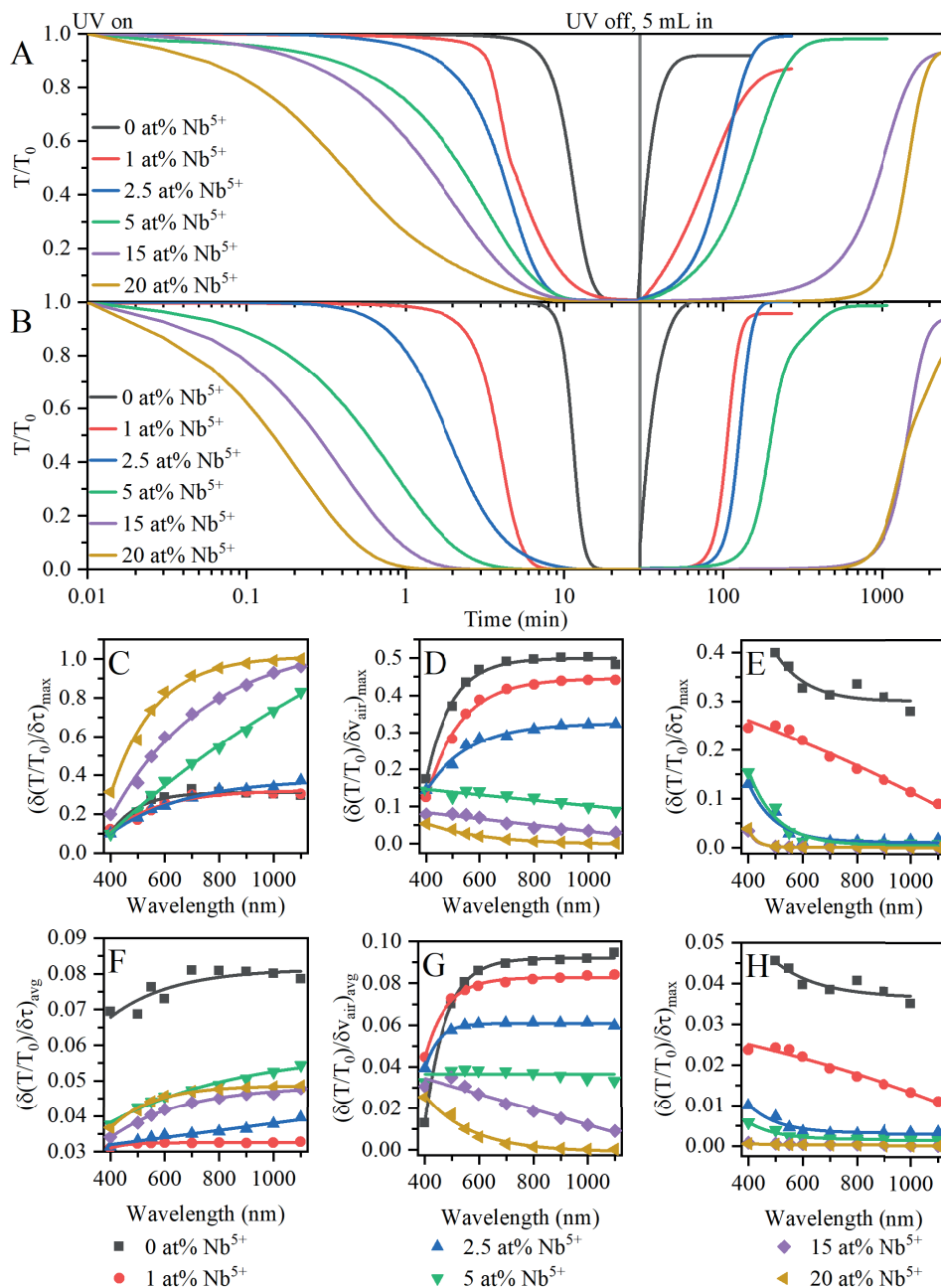


Fig. 3.15. T/T_0 plots of the transmittance change during UV irradiation and subsequent steady state recovery at A – 550 nm; B – 1000 nm; C, D, E – maximum relative transmittance change rate for photodarkening (C); dynamic recovery (D) and steady-state recovery (E); F, G, H – average relative transmittance change rate of photodarkening (F); dynamic recovery (G); steady-state recovery (H).

A similar picture is seen when looking at the steady state recovery rates (Fig. 3.15 A, B). Here the un-doped TiO_2 sample after 5 mL of air recovered relatively rapidly, in only 25 min.

This is largely due to the fact that 5 mL is very close to the amount of air necessary to achieve recovery in the dynamic experiment. In both the visible (550 nm) and NIR (1000 nm) ranges, the un-doped TiO₂ nanoparticle colloid showed a similar recovery, owing to the easily quenchable nature of the Ti³⁺ and V_O^{••} defects. All the Nb⁵⁺ samples, on the other hand, required at least 3 times the amount of time to recover (1 at% Nb⁵⁺ sample required 76 min to recover in the NIR range). This time was exponentially longer for the 15 at% and 20 at% sample colloids (around 35 hours) to recover in the visible range and even longer (40–48 hours) to recover in the NIR range. This can be attributed to multiple effects. First, the slow initial recovery can be attributed to the correlation of transmittance and absorbance at low transmission values. In this regime, large changes in absorbance result in only marginal changes transmittance. The second effect is due to the more stable Nb⁴⁺-V_O-Ti⁴⁺ complex defect. The relative transmittance change was derived by time, resulting the relative transmittance change rate for not only the photodarkening (Fig. 3.15 C, F) but also the dynamic (Fig. 3.15 D, G) and steady-state recovery rates (Fig. 3.15 E, H). The steady-state recovery rates had a much wider spread depending on the Nb⁵⁺ content. The difference between the un-doped and 20 at% Nb⁵⁺ doped TiO₂ colloids was more than 2 orders of magnitude (359 times) at 700 nm for the maximum recovery rate and similar difference also for the average recovery rate. As a higher stability of the defects leads to an increased formation rate and a decreased annihilation rate, this theory correlates neatly with the observed results. To make the Nb⁵⁺ doped TiO₂ nanoparticle colloids more suitable for practical applications, the recovery rate needs to be increased. Taking inspiration from the previous research on TiO₂ colloids in different solvents, one possibility for the increase in the recovery can be the usage of an ethanolamine additive. For that purpose, the colloids of 20 at% Nb⁵⁺ doped TiO₂ nanoparticles were modified with varying amounts of TEOA (25, 50 and 100 mol% with respect to the amount of TiO₂ present, Fig. 3.16). The steady-state recovery rate for colloids containing 25 mol% TEOA in both wavelength ranges recovered 7.42 times faster – in 330 min. It is worth noting, that the recovery in case of TEOA addition was observed with no air injection. If air was additionally injected, this would further increase the recovery rate, similarly as was observed for the un-doped TiO₂ colloids.

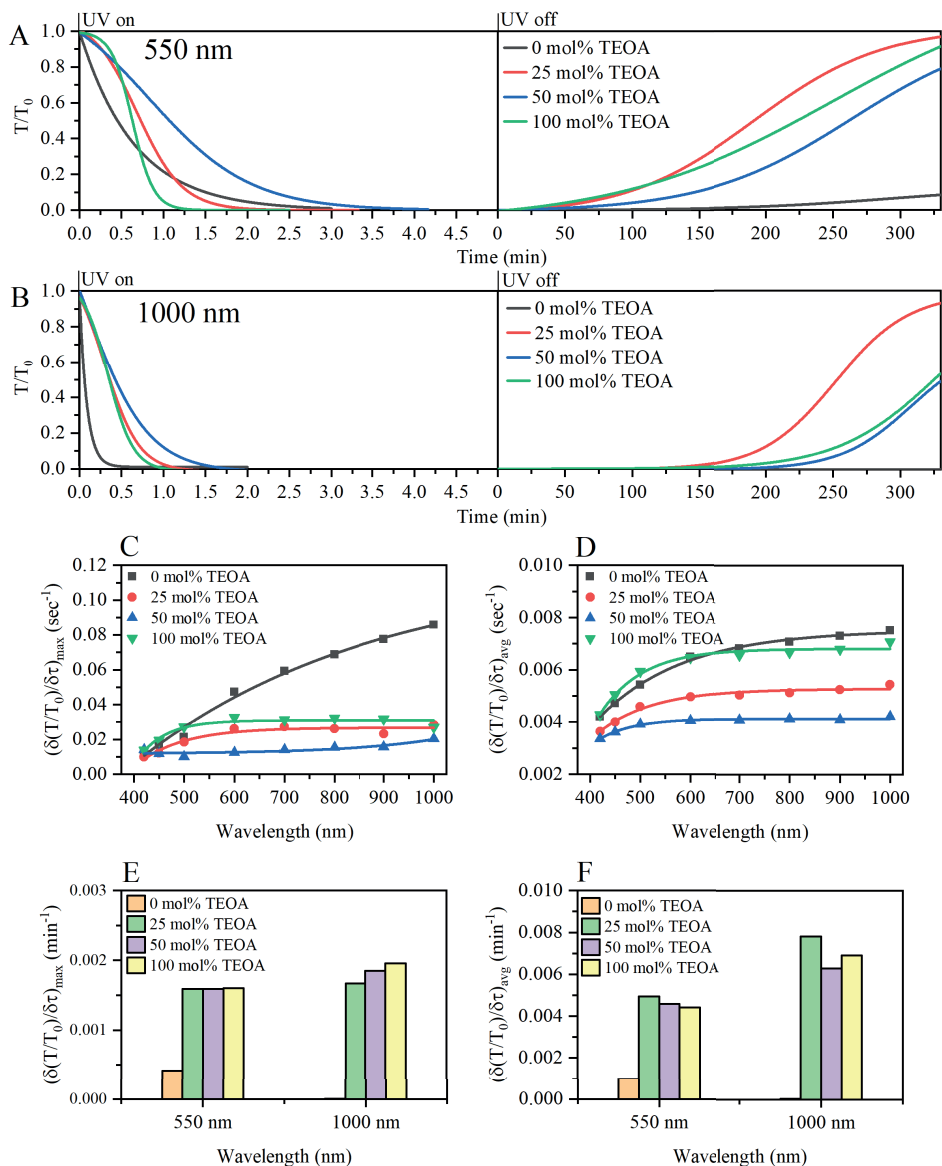


Fig. 3.16. T/T_0 plots during UV irradiation and airless recovery for the colloid of 20% Nb-doped TiO₂ with the addition of triethanolamine (different mol% relative to the amount of TiO₂ for A – 550 nm; B – 1000 nm; C – maximum photodarkening rate and D – average photodarkening rate for Nb⁵⁺-doped TiO₂ colloid without and with 25, 50 and 100 mol% TEA additive; E – maximum recovery rate of the colloids without air injection at 550 and 1000 nm; F – average recovery rate of the colloids without air injection at 550 and 1000 nm.

As mentioned previously, the dramatic increase in the photodarkening rate of the Nb⁵⁺-doped TiO₂ colloids when compared to pristine TiO₂ stems from the formation of the complex point defect Nb⁴⁺-V_O-Ti⁴⁺. The evidence for this can be gathered from EPR experiments. EPR spectroscopy was done for the Nb⁵⁺ doped TiO₂ colloid sample with the highest Nb content of 20 at% (Fig. 3.17). Before UV irradiation, we observe the same three

signals as for the un-doped TiO₂ colloid. However, there is no evidence of a Ti³⁺ signal either during or after UV irradiation. Instead, a new spectral feature with a g-value of 1.977 and $\Delta H = 4$ G was detected, and its intensity was seen to increase with irradiation time. This signal can be attributed to Nb⁴⁺, to be precise, the defect model of Nb⁴⁺-V_O-Ti⁴⁺.⁵¹ Although the Nb⁴⁺ signal cannot be seen in EPR at temperatures above 77K, because of the complex defect configuration, detection of the signal was permitted above 77K at room temperature. The results indicate that the Nb doped TiO₂ contain different point defects responsible for photochromism when compared to un-doped TiO₂. When calculating the number of defects, it was observed that the number of defects reached saturation already after 30 min, instead of the 60 min for un-doped TiO₂. This observation agrees with our UV-Vis spectroscopy results that show a higher photodarkening rate for samples doped with Nb⁵⁺.

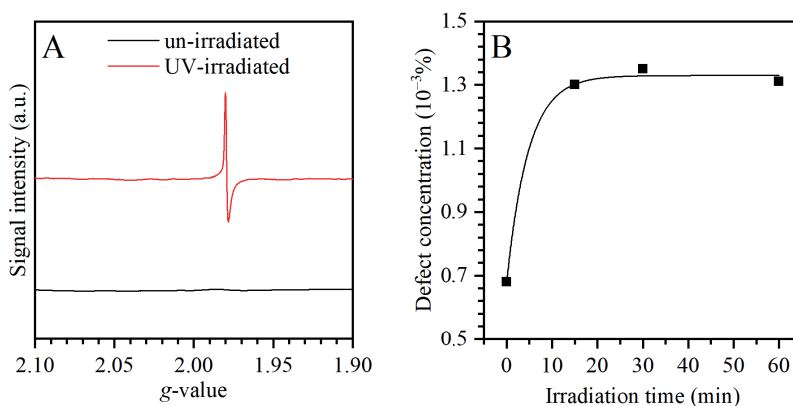


Fig. 3.17. A – EPR spectra for the 20 at% Nb⁵⁺ doped TiO₂ nanoparticle colloid before and after UV irradiation; B – the relevant defect concentrations as a function of irradiation time.

3.5. Photochromic TiO₂ polymer gels

The TiO₂ nanoparticles suspended in a hole scavenging media is a potent material for photochromic applications. However, for most real-life applications, colloids are not usable, as they are prone to leakage from most closed systems and can evaporate, causing a pressure increase, which can potentially ruin the closed system. Thin films, however, have a much lower absorptivity, cause to achieve the equivalent absorption to the colloids, a film with a thickness of at least 8 μm is necessary. Films that thick are difficult to produce. Furthermore, when films are this thick, the hole scavenger can only interact with the upper layer of the films. Thus, photodoping happens only on the top layer and basically makes thin film usage impossible. The middle ground for combining the potential of colloids with the stability of thin films would be gels, as these would allow to produce closed systems, which are much less prone to evaporation and leakage while allowing hole scavenging to happen through the hole gel volume. The gels presented here are transparent in the undarkened state while absorbing almost all the light in the photodarkened state. These gels also have a performance, comparable to the colloid samples discussed earlier. The gels form the PEGDA polymer by photocrosslinking with the help of the TiO₂ nanoparticles (Fig. 3.18 A). TiO₂ acts as a photoinitiator for the crosslinking process,

resulting in the polymerization of PEGDA via the vinyl terminal groups. To keep the gels stable and transparent, DMF was necessary. A large variety of gel compositions were made under this study, and an approximation of a compositional diagram can be made (Fig. 3.18 B). We can see that if the PEGDA content is below 5 vol%, gel formation is not expected. This, however, is not quite the case as if the TiO₂ content is above 17 vol%, the samples were gels, even without PEGDA. Sadly, these gels have hardly any photochromic activity, as DMF is not known to be a hole scavenger, and as such the photodoping effect is severely diminished. Additionally, the influence of ethanol on the photochromic performance of these gels was examined.

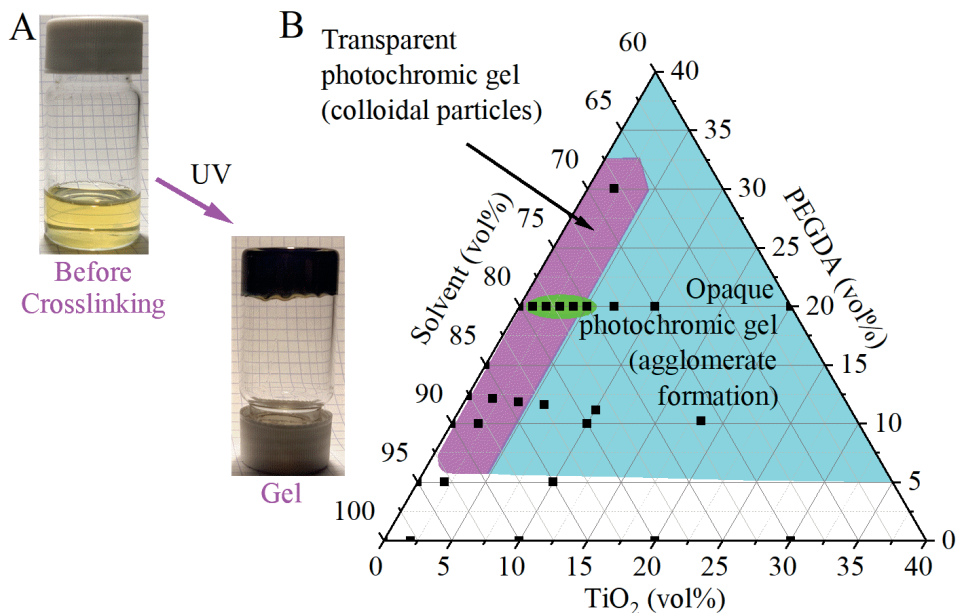


Fig. 3.18. A – photograph of a TiO₂ / PEGDA gel composition (3 vol% TiO₂ and 20 vol% EtOH) before and after UV irradiation; B – ternary diagram displaying the compositional range where the transparent and opaque gels are obtained (white region indicates no gel formation). Green circle indicates the region of compositions studied further.

The transmittance changes between the initial and photodarkened states was dependent on the TiO₂ content as well as on the amount of EtOH present in the gels. The highest amount of variation in the transmittance change was for the samples without EtOH. Here, the transmittance change varied from 11.2 % for the sample with 1 vol% of TiO₂ at 400 nm to 89.8 % for the sample with 5 vol% TiO₂ at 700 nm (Fig. 3.19 A). The transmittance change dependence on the TiO₂ content was linear for low to medium TiO₂ contents (1–3 vol%), while for higher TiO₂ contents (4–5 vol%) the transmittance change was decreased. This can be explained by several reasons. First, the diminishing returns can be explained by the correlations between absorbance and transmittance. This correlation is logarithmic, meaning that when the absorbance is low, small changes in absorbance lead to large changes in transmittance. Subsequently, when the absorbance is high, even large changes in absorbance can lead to relatively small changes in transmittance. Another possibility is that this is mainly due to saturation. This is also the reason why Lambert's law can be applied only for low concentrations.

When EtOH was added to the samples, an increase in the transmittance change was observed with a maximum transmittance change seen at 700 nm (Fig. 3.19 B–D). The increase in the absolute transmittance change is due to the nature of ethanol being a very potent hole scavenger, as was seen previously. This, in turn, allowed for a greater number of electrons to accumulate in the nanoparticles, both as delocalized electrons in the conduction band as well as in the form of Ti^{3+} defects. The presence of EtOH gradually increased the transmittance change, with samples with a lower TiO_2 content (1–3 vol%) benefiting more than samples with a higher TiO_2 content (4–5 vol%). This is again due to saturation. However, the presence of EtOH (30 vol%) allowed the low TiO_2 content (1–2 vol%) samples to achieve a transmittance change of over 80 %.

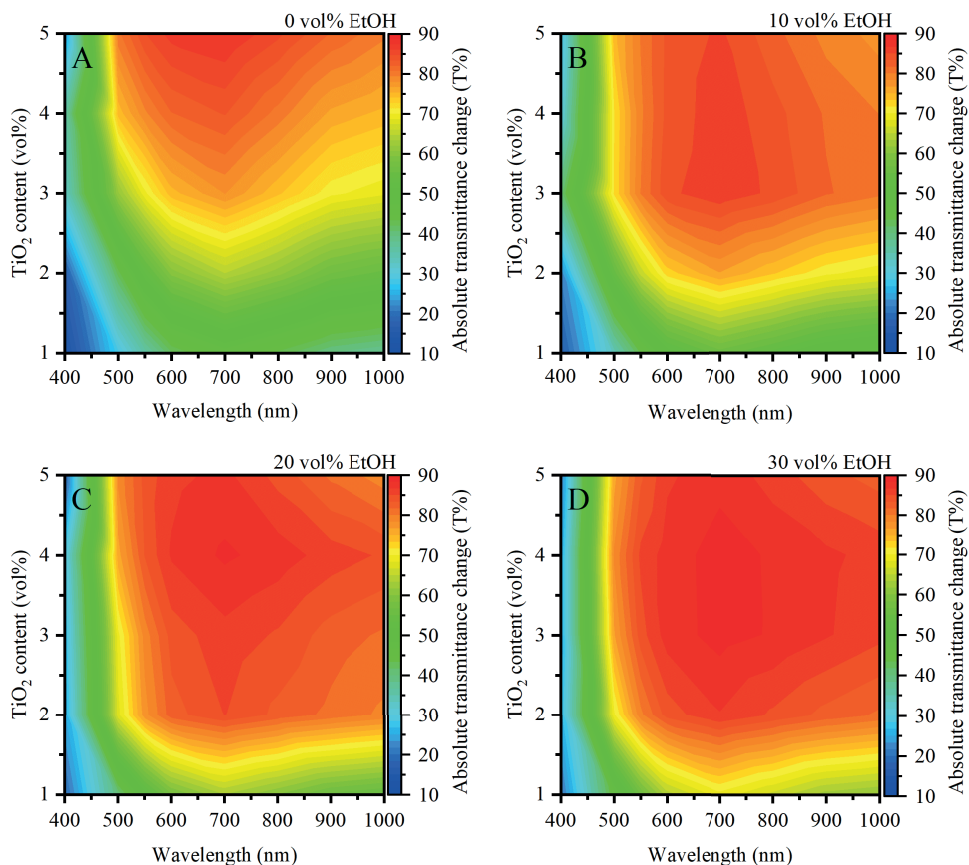


Fig. 3.19. Absolute transmittance change of the samples with different TiO_2 contents and at different wavelengths for samples with a EtOH content of A – 0 vol%; B – 10 vol%; C – 20 vol%; D – 30 vol%.

The increase in absolute transmittance change also is indicative of a metastable system, as recovery takes place all the time, just very slowly. Without ethanol, the photodarkening and recovery reach an equilibrium at a lower absorption. Ethanol, acting as a catalyst, shifts this equilibrium towards a higher absorption. Evidence for this can also be seen in the transmittance change rate. Without ethanol (Fig. 3.20 A) the samples photodarkened very slowly, requiring

120 min to reach saturation. This resulted in change rates of as low as $-1.6 \times 10^{-2} \text{ min}^{-1}$ for 1 vol% TiO_2 sample at 400 nm to as high as -0.93 min^{-1} for 5 vol% TiO_2 samples at 400 nm. Here, the large apparent photodarkening rate of the sample with 5 vol% of TiO_2 was the result of multiple simultaneous processes. First, the photodarkening was taking place similarly to the rest of the samples. However, another process that took place was the agglomeration of the nanoparticles. This led to scattering that further decreased the transmittance of the gel samples. Evidence of this was the fact that the high photodarkening rate was mainly seen for shorter wavelengths (400–550 nm) that are susceptible to scattering from smaller agglomerates than for longer wavelengths as per Mie scattering theory. For all other samples the photodarkening rate was the highest at 700 nm.

When ethanol was added to the composition, the result was a general increase in the photodarkening rate, that was also evident from the fact that the samples needed to be irradiated only for 30 min instead of 120 min for saturation. Further irradiation did not result in any noticeable increase in absorption. The photodarkening rate increased the most when the ethanol content was increased from 0–10 vol% (Fig. 3.20 B). Samples with a low TiO_2 content of 1–2 vol% exhibited a slightly higher increase (362 % on average) when compared to samples with a higher TiO_2 content of 3–4 vol% (248 % on average). The sample with a TiO_2 content of 5 vol% exhibited a very slight increase in the photodarkening rate of just 29 % on average, mainly due to the already high photodarkening rate. This comparatively negligible photodarkening rate increase, when compared to the rest of the samples, shows that scattering effects, taking place due to agglomeration, are the main causes for the high photodarkening rate. When the ethanol content was increased further, the results were a lot less pronounced. An increase in the photodarkening rate of just 6 % on average was observed when the ethanol content was increased from 10 vol% to 20 vol% (Fig. 3.20 C), with a further 10 % on average observed when the ethanol content was increased by an addition 10 vol% to 30 vol% in total (Fig. 3.20 D). Here again, the highest 29 % increase was for the samples with a low TiO_2 content of 1–2 vol%, while the photodarkening rate increased just by 2 % on average for higher TiO_2 content samples. With the maximum amount of ethanol this resulted in photodarkening rates ranging from $-7.9 \times 10^{-2} \text{ min}^{-1}$ to $-5.2 \times 10^{-1} \text{ min}^{-1}$, which was a total increase of 465 % on average for the samples with a low TiO_2 content of 1–2 vol%. The diminishing returns for subsequent increases in ethanol show, that with even 10 vol%, have almost all of the possible adsorption sites covered, i.e., the nanoparticle surface is almost saturated with ethanol and during photodarkening, the TiO_2 nanoparticles give out holes (the ethanol scavenges the holes) at almost the maximum rate, which is limited by the processes of ethanol adsorption, electron migration and subsequent aldehyde desorption.

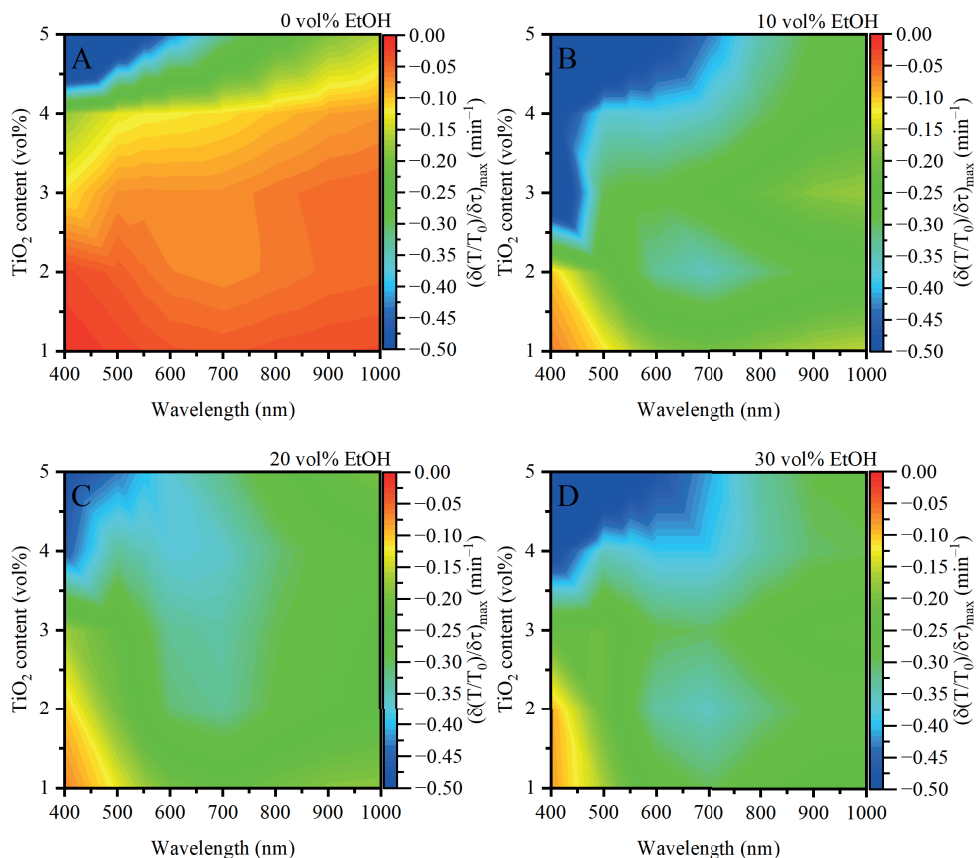


Fig. 3.20. Photodarkening kinetics of the samples with different TiO_2 contents and at different wavelengths for samples with a EtOH content of A – 0 vol%; B – 10 vol%; C – 20 vol%; D – 30 vol%.

The samples recovered when the UV light was turned off. The recovery was much slower, with an average recovery rate in the order of magnitude of from $2.4 \times 10^{-5} \text{ min}^{-1}$ to $2.2 \times 10^{-3} \text{ min}^{-1}$, with the highest recovery rate for the 3 vol% TiO_2 sample at the NIR range (Fig. 3.21 A). The slowest recovery was for the sample with the highest TiO_2 of 5 vol%. This is due to the fact that the more photodoped TiO_2 is present in the sample, the more recovery needs to take place. In this case the recovery is done through the photoreduction of the oxidized species present in the gel. The photoreduction takes place because the nanoparticles have a large accumulation of electrons. These electrons are then capable of reducing organic species in the gel, which have previously been oxidized.

When 10 vol% of ethanol is added to the samples, the recovery rate increases by 90 % on average (Fig. 3.21 B). Here, the highest increase in recovery rate is seen again for samples with a low TiO_2 of 1–2 vol%, with an increase of 139 %. The sample with the lowest TiO_2 content studied of just 1 vol% exhibited an increase in the recovery rate of 204 % on average, increasing the recovery rate from $1.2 \times 10^{-3} \text{ min}^{-1}$ to $3.8 \times 10^{-3} \text{ min}^{-1}$ at 550 nm and from $1.4 \times 10^{-3} \text{ min}^{-1}$ to $4.2 \times 10^{-3} \text{ min}^{-1}$ at 1000 nm. All the rest of the samples showed a much lower increase in the recovery rate of just 62 % on average. A further increase in the ethanol

content of 10 vol% (20 vol% in total Fig. 3.21 C) resulted in a further 43 % increase in the recovery rate, with a lot more even increase across the studied samples. The highest recovery rate was observed for the samples with a low TiO₂ content (1–2 vol%) with values of $4.2 \times 10^{-3} \text{ min}^{-1}$ at 550 nm and $4.9 \times 10^{-3} \text{ min}^{-1}$ at 1000 nm for the sample with a TiO₂ content of 1 vol% and $3.4 \times 10^{-3} \text{ min}^{-1}$ at 550 nm and $3.3 \times 10^{-3} \text{ min}^{-1}$ at 1000 nm for the sample with a TiO₂ content of 2 vol%. Further increasing the ethanol content to 30 vol% (Fig. 3.21 D) led to an average increase of 33 % across all the samples with the highest increase observed for the samples with a high TiO₂ content. The highest overall increase was observed for the samples with a TiO₂ content of 2 and 3 vol%, with the 3 vol% sample reaching a recovery rate of $5.6 \times 10^{-3} \text{ min}^{-1}$ at 550 nm and $4.4 \times 10^{-3} \text{ min}^{-1}$ at 1000 nm.

The gradual increase in the recovery rate with ethanol addition was due to the nature of the oxidation products. When ethanol is present in the gels, during hole scavenging, the by products are acetaldehyde or even acetic acid. With the photodoped TiO₂ nanoparticles, acetaldehyde can be photoreduced back to ethanol with the interaction with the accumulated electrons. This is done easier than the photoreduction of the other potential photooxidation products possible, such as oxidation products of acetylacetonate, PEGDA or DMF. This is also of note, because the photooxidation of these molecules can be accompanied by the cleavage of bonds, resulting in an irreversible oxidation reaction. Acetylacetonate can be oxidized to acetic acid and formic acid via Baeyer-Villiger oxidation.⁵² PEGDA has multiple fragments in its molecule, which are prone to possible oxidation reactions such as the carboxy fragments at the ends as well as ethylene glycol fragments in the middle of the molecule.⁵³ DMF is susceptible to oxidation, with the help of hydroxyl groups that could easily be introduced into the system from the TiO₂ surface.⁵⁴ This oxidation is also accompanied by the cleavage of a C-N bond, resulting in demethylation of the DMF molecule. On the other hand, acetaldehyde could be photoreduced back to ethanol, as it has been shown that aldehydes can be reduced with the help of TiO₂ under UV irradiation, acting as electron scavengers.^{55–57}

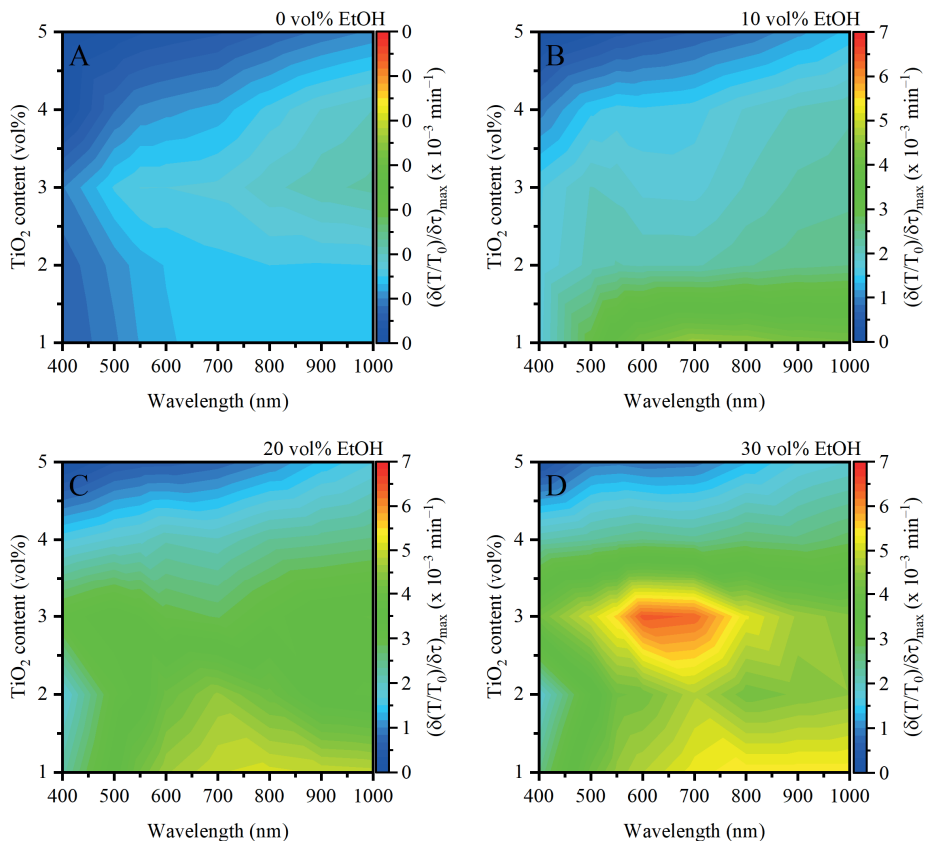


Fig. 3.21. Recovery kinetics of the samples with different TiO₂ contents and at different wavelengths for samples with a EtOH content of A – 0 vol%; B – 10 vol%; C – 20 vol%; D – 30 vol%.

For samples without ethanol (Fig. 3.22 A) with a TiO₂ content above 1 vol%, the recovery is incomplete, especially in the shorter wavelength range. The sample with 2 vol% TiO₂ showed a recovery effectiveness of 86.6 % at 400 nm, which gradually increased with increasing wavelength and at 600 nm reached full recovery of 99.2 %. The sample with 3 vol% TiO₂ recovered only 24.2 % at 400 nm with a gradual increase in recovery up to 97 % at 1000 nm. The samples with a higher TiO₂ (4–5 vol%) did not recover, with the 4 vol% sample recovering to just 92.5 % at 1000 nm and the 5 vol% sample recovering to just 81.5 % at 1000 nm. The reason for this limited recovery is that without a dedicated hole scavenger the gels themselves start to degrade during the photodarkening process and scattering starts to occur. This is indicated by the recovery efficiency being higher at longer wavelengths when comparing to shorter ones.

When 10 vol% of ethanol is introduced into the samples (Fig. 3.22 B), the recovery shows a noticeable increase across all the samples. The 2 vol% TiO₂ sample now recovers fully even at 400 nm with a recovery effectiveness between 97.8 % and 100 %. The samples with a higher TiO₂ content exhibit and increase in recovery effectiveness of 9 % on average in the NIR wavelength range of 700–1100 nm and 20 % on average in the visible range (400–600 nm)

when compared to the samples without ethanol. The highest increase in the recovery effectiveness was observed for the sample with 4 vol% TiO₂ with an increase in recovery effectiveness of 30 % at 550 nm. This drastic increase in the recovery effectiveness of the samples with the introduction of ethanol even at 10 vol% shows that when a dedicated hole scavenger is present in the system, the rest of the constituents are spared from the photooxidation happening when photodarkening occurs. This allows for the stability to be kept and scattering caused by agglomeration – avoided. An increase in the ethanol content to 20 vol% (Fig. 3.22 C) resulted in a very slight (~1 %) increase in the recovery effectiveness overall when compared to samples with 10 vol% ethanol, with a more noticeable increase in the recovery of the 3 vol% TiO₂ sample at 400 nm (from 31.8 % to 40.6 %). When the ethanol content was increased to 30 vol% (Fig. 3.22 D), there was a more noticeable increase in the recovery effectiveness, with the mayor increase being for the sample with 3 vol% TiO₂. This sample exhibited an increase in recovery effectiveness of 49.3 % at 400 nm and 7.7 % at 550 nm, bringing its total recovery effectiveness up to 89.9 % at 400 nm and full recovery (98 + %) at the wavelength range of 600–1100 nm. The samples with a high TiO₂ content of 4–5 vol% exhibited an overall increase in the recovery effectiveness of 30.4 % and 18.6 % in the visible range (400–600 nm) and 9.3 % and 14.4 % in the NIR range for the samples with 4 vol% and 5 vol% TiO₂, respectively.

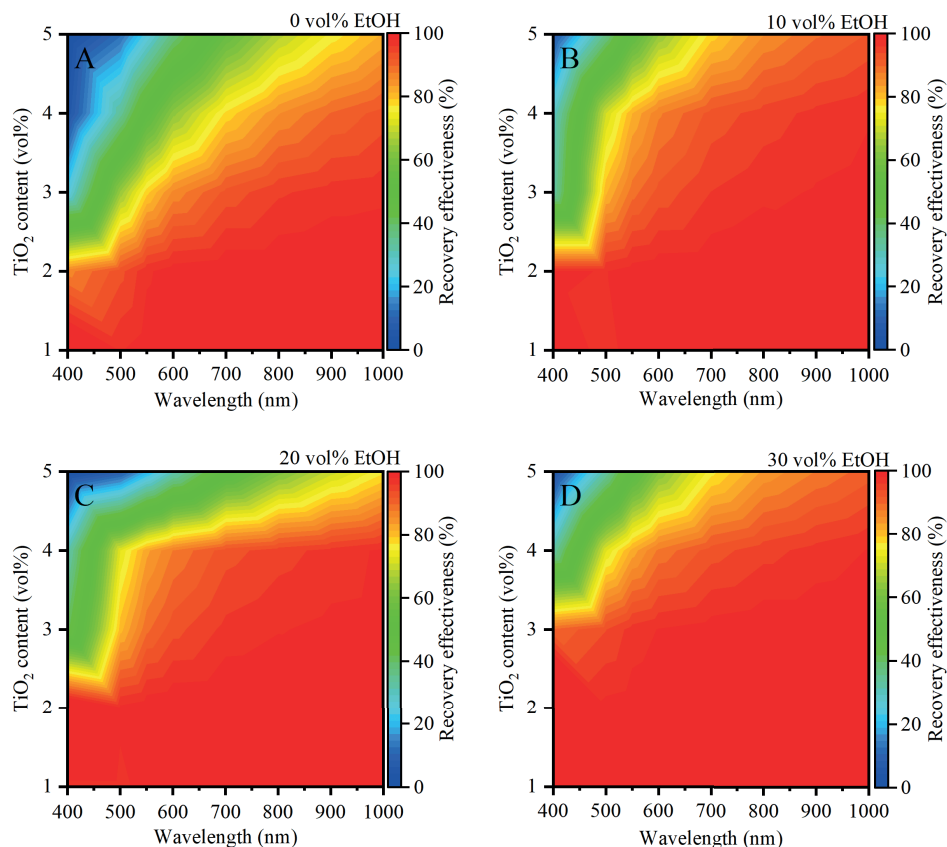


Fig. 3.22. Recovery effectiveness (%) of the samples with different TiO_2 contents and at different wavelengths for samples with EtOH content of A – 0 vol%; B – 10 vol%; C – 20 vol%; D – 30 vol%.

The fact that even with 30 vol% of ethanol the samples with a high TiO_2 content (>3 vol%) did not recover fully would suggest that there is need to continue the increase of the amount of ethanol. After all, only at 30 vol% ethanol content did the sample with 3 vol% TiO_2 started to exhibit a full recovery. The amount of ethanol usable in the composition is limited. When experimenting with higher ethanol contents for samples with a TiO_2 content of 2 vol% (Fig. 3.23 A) the upper limit for the ethanol content is between 40–50 vol%. Already at 40 vol% the sample exhibited a slight decrease in the recovery of between 0–2 % in the visible wavelength range. At 50 vol% the sample exhibited a more pronounced decrease in the recovery effectiveness of the gel, with a decrease in recovery of between 2.8–6.8 % in the visible range. In both cases the recovery in the NIR wavelength range was unchanged. However, when the ethanol content was increased above 50 vol% (to 60 vol%), the samples recovery drastically decreased to just 5.9 % on average, with an average recovery of just 1.4 % in the visible range. This, in essence, meant that the gel system is no longer stable. The reason for this is the fact that ethanol replaces DMF in the composition. With an increase in the ethanol content the DMF content is reduced proportionally. As DMF is the stabilizer in the system, at least a minimum amount is needed to keep the gel/nanoparticle network stable. From these observations it can

be concluded that a minimum nanoparticle to DMF volume ratio of 1 : 10 should be used, to keep the gel transparent.

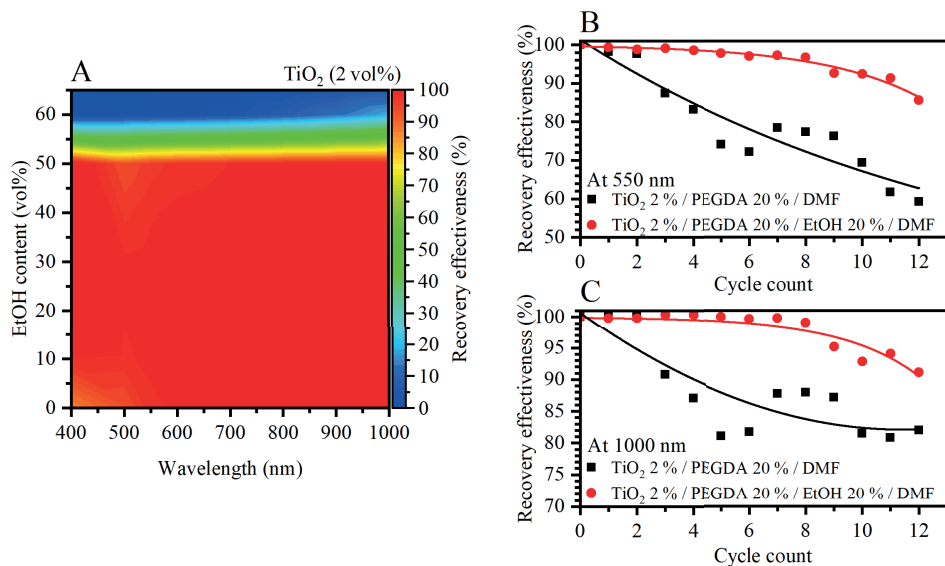


Fig. 3.23. A – recovery effectiveness of samples with a TiO₂ content of 2 vol% and different amounts of ethanol at different wavelengths; B – transmittance recovery during subsequent UV irradiation/recovery cycles at 550 nm for samples with and without EtOH; C – transmittance recovery during subsequent UV irradiation/recovery cycles at 1000 nm for samples with and without EtOH.

Lastly, we investigated the cycling stability of the photochromic gels. The stability was tested for 12 photodarkening-recovery cycles by repeatedly irradiating samples with a TiO₂ content of 2 vol% (samples without EtOH 120 min, samples with 20 vol% EtOH 30 min) and allowing them to recover. The recovery in visible and NIR ranges was different with gels being stable for longer in the NIR range when compared to the visible. In the visible range (Fig. 3.23 B) the transmittance recovery in response to UV gradually decreases cycle over cycle, with the sample with 20 vol% EtOH decreasing from 99 % in the 1st cycle to 92 % after the 10th cycle and the sample without EtOH decreasing from 98 % in the 1st cycle to just 69 % in the 10th cycle. This resulted in a recovery effectiveness decrease of 7 % and 29 % for the samples with and without EtOH, respectively. In the NIR region (Fig. 3.23 C) the samples showed a much better recovery from cycle to cycle, especially with the 20 vol% EtOH addition with the transmittance recovery decreasing from an initial 100 % in the 1st cycle to 93 % in the 10th cycle. The sample without EtOH showed a recovery efficiency decrease of 18 % over 10 cycles, from 100 % in the 1st cycle to 82 % in the 10th. The difference between the visible and NIR ranges stems from the fact that shorter wavelengths are more susceptible to the scattering caused by agglomeration and scatter on smaller size agglomerates as per Mie theory^{58,59}. This can also be explained by the fact that the Ti³⁺ and oxygen vacancy defects created under the TiO₂ QD surface are stable and recover slowly because point defects migrate slower than electrons. Also, it is worth pointing out that for both vis and NIR spectral range the recovered transmittance for the sample with 20 vol% EtOH after each cycle was fairly constant and only started no

noticeably drop after 8 cycles (at 550 nm 91% in the 1st and 88 % in the 8th cycle, at 1000 nm 90 % in the 1st, and 89 % after the 8th cycle) as opposed to the sample without ethanol, which had a drop in the recovered transmittance after just 3 cycles (at 550 nm from 91 % in the 1st cycle, 90 % in the 3rd, and 70 % after the 8th cycle and at 1000 nm 90 % in the 1st and 3rd cycle and 79 % after the 8th cycle). This shows that the addition of EtOH had a positive impact not only on the photodarkening intensity and rate as well as the recovery effectiveness and rate, but also on the stability of the system. This also is due to the fact that EtOH, acting as the hole scavenger, allows the rest of the constituents (DMF and crosslinked PEGDA) to remain untouched, thus making the gel more stable. Also, it means that photooxidation products can be photoreduced on photodoped TiO₂ QDs to facilitate better recovery.

Conclusions

1. Titanium dioxide has been found to exhibit photochromism in a variety of different hole scavenging solvents, such as primary and secondary alcohols. The highest photochromic response has been found to be for primary alcohols, with colloids in ethanol having the highest photochromic response. This is due to the unstable nature of the ethanol oxidation products allowing for rapid adsorption/hole scavenging/desorption to happen on the nanoparticle surface.
2. The addition of ethanolamines increased the recovery, allowing the colloids to recover their transmittance in a fraction of the time, when compared to colloids without ethanolamines. However, this also had a negative effect on the photodarkening of titanium dioxide. This is because ethanolamines can oxidize to nitrocompounds, which can in turn scavenge the photoaccumulated electrons during photodarkening.
3. The change in charge carrier concentration can be measured as a change in electrical resistivity for nanoparticle thin films that are too thin to measure their change in transmittance spectroscopically. This resistivity change was observed when the thin films were exposed to hole scavenger vapors similarly to particles suspended in hole scavengers. This has the potential of being used for alcohol vapor gas sensing.
4. The electron photoaccumulation can be used for electricity generation and its photostorage by using a photoelectric device. Thin films can be charged in 5 min allowing to obtain a power output of $0.0203 \mu\text{W}/\text{cm}^2$. This shows that the photochromic effect can be also used further, not only for light modulation but also to supply power to low-powered sensors in remote locations.
5. Successful doping of titanium dioxide with niobium was prepared by subsequent solvothermal treatment, which resulted in high doping efficiency of 99–100 % up to a dopant amount of 20 at%. No secondary phase formation was seen with distortions of the anatase crystalline lattice being observed by the introduction of the slightly larger Nb^{5+} cations. This resulted in a decrease in the optical band gap, which can be attributed to the formation of acceptor defect near the conduction band minimum.
6. The Nb^{5+} doped titanium dioxide exhibited a strong increase in the photochromic kinetics. The Nb^{5+} defects allowed for rapid photochromism, with 20 at% of niobium resulting in an order of magnitude increase in the photochromism speed photodarkening in just 1 minute, comparing to 20 minutes required for the un-doped nanoparticles in the same conditions. Due to the nature of the Nb^{5+} traps, this also resulted in an increased recovery time, requiring almost 2 days to recover, comparing to just 30 minutes for the un-doped nanoparticle colloids. The main type of defects in these nanoparticles were $\text{Nb}^{4+}\text{-V}_\text{O}\text{-Ti}^{4+}$, while without Nb^{5+} , the main defects were Ti^{3+} .
7. The un-doped titanium dioxide was successfully incorporated into transparent polymeric gels comprised of polyethylene glycol diacrylate and *N,N*-dimethylformamide. The transparency was retained because of the stabilizing properties of *N,N*-dimethylformamide. The amount of titanium dioxide had to be kept between 1–4 vol% to retain transparency, and at least 10 vol% of polyethylene glycol diacrylate was needed to produce a gel.
8. The partial substitution of *N,N*-dimethylformamide with ethanol allowed for a dramatic increase in both the photodarkening and recovery speed. This also resulted in an increase of the stability of the prepared gel due to ethanol taking over the role as the main hole

scavenger, thus protecting the remaining constituents from oxidation. This allowed the gel to remain transparent in its undarkened state for longer, withstanding 8 photodarkening/recovery cycles, without noticeable degradation.

REFERENCES

- 1 D. T. Gillaspie, R. C. Tenent and A. C. Dillon, Metal-oxide films for electrochromic applications: Present technology and future directions, *Journal of Materials Chemistry*, 2010, **20**, 9585–9592.
- 2 Y. Badour, V. Jubera, I. Andron, C. Frayret, and M. Gaudon, Photochromism in inorganic crystallised compounds, *Optical Materials: X*, 2021, **12**, 100110.
- 3 V. A. Barachevsky, Negative photochromism in organic systems, *Review Journal of Chemistry*, 2017, **7**, 334–371.
- 4 Z. Gao, L. Liu, Z. Tian, Z. Feng, B. Jiang, and W. Wang, Fast-Response Flexible Photochromic Gels for Self-Erasing Rewritable Media and Colorimetric Oxygen Indicator Applications, *ACS Applied Materials and Interfaces*, DOI:10.1016/j.jbiomech.2005.02.020.
- 5 P. Nyamukamba, O. Okoh, H. Mungondori, R. Taziwa, and S. Zinya, in *Titanium Dioxide – Material for a Sustainable Environment*, InTech, 2018.
- 6 T. Hachisu, K. Shi, T. Yokoshima, A. Sugiyama, S. Kuroiwa, T. Osaka, N. Nakajima, and M. Yoshino, Preparation of anatase phase titanium dioxide film by non-aqueous electrodeposition, *Electrochemistry Communications*, 2016, **65**, 5–8.
- 7 T. Cottineau, L. Brohan, M. Pregelj, P. Cevc, M. Richard-Plouet, and D. Arçon, Evidence of interfacial charge transfer upon UV-light irradiation in novel titanium oxide gel, *Advanced Functional Materials*, 2008, **18**, 2602–2610.
- 8 P. Szymanski and M. A. El-Sayed, Some recent developments in photoelectrochemical water splitting using nanostructured TiO₂: a short review, *Theoretical Chemistry Accounts*, 2012, **131**, 1202.
- 9 H. Dürr, in *Photochromism*, Elsevier, 2003, pp. 1–14.
- 10 V. Likodimos, C. Han, M. Pelaez, A. G. Kontos, G. Liu, D. Zhu, S. Liao, A. A. de la Cruz, K. O’Shea, P. S. M. Dunlop, J. A. Byrne, D. D. Dionysiou, and P. Falaras, Anion-Doped TiO₂ Nanocatalysts for Water Purification under Visible Light, *Industrial & Engineering Chemistry Research*, 2013, **52**, 13957–13964.
- 11 U. Joost, A. Šutka, M. Oja, K. Smits, N. Döbelin, A. Loot, M. Järvekülg, M. Hirsimäki, M. Valden, and E. Nömmiste, Reversible Photodoping of TiO₂ Nanoparticles for Photochromic Applications, *Chemistry of Materials*, 2018, **30**, 8968–8974.
- 12 D. K. Diop, L. Simonot, J. Martínez-García, M. Hébert, Y. Lefkir, G. Abadias, P. Guérin, D. Babonneau, and N. Destouches, Spectral and Color Changes of Ag/TiO₂ Photochromic Films Deposited on Diffusing Paper and Transparent Flexible Plastic Substrates, *Applied Spectroscopy*, 2017, **71**, 1271–1279.
- 13 J. J. Carey and K. P. McKenna, Screening Doping Strategies to Mitigate Electron Trapping at Anatase TiO₂ Surfaces, *Journal of Physical Chemistry C*, 2019, **123**, 22358–22367.
- 14 U. Joost, A. Šutka, M. Oja, K. Smits, N. Döbelin, A. Loot, M. Järvekülg, M. Hirsimäki, M. Valden, and E. Nömmiste, Reversible Photodoping of TiO₂ Nanoparticles for Photochromic Applications, *Chemistry of Materials*, 2018, **30**, 8968–8974.

- 15 F. Paquin, J. Rivnay, A. Salleo, N. Stingelin, and C. Silva, Multi-phase semicrystalline microstructures drive exciton dissociation in neat plastic semiconductors, *J. Mater. Chem. C*, 2015, **3**, 10715–10722.
- 16 H. Zhang, R. Shi, A. Xie, J. Li, L. Chen, P. Chen, S. Li, F. Huang, and Y. Shen, Novel TiO₂/PEGDA hybrid hydrogel prepared in situ on tumor cells for effective photodynamic therapy, *ACS Applied Materials and Interfaces*, 2013, **5**, 12317–12322.
- 17 C. di Valentin and D. Fittipaldi, Hole scavenging by organic adsorbates on the TiO₂ surface: A DFT model study, *Journal of Physical Chemistry Letters*, 2013, **4**, 1901–1906.
- 18 N. Serpone, D. Lawless, R. Khairutdinov, and E. Pelizzetti, Subnanosecond Relaxation Dynamics in TiO₂ Colloidal Sols, *Journal of Physical Chemistry*, 1995, **99**, 16655–16661.
- 19 T. Tachikawa, Y. Takai, S. Tojo, M. Fujitsuka, and T. Majima, Probing the surface adsorption and photocatalytic degradation of catechols on TiO₂ by solid-state NMR spectroscopy, *Langmuir*, 2006, **22**, 893–896.
- 20 I. Nakamura, N. Negishi, S. Kutsuna, T. Ihara, S. Sugihara, and K. Takeuchi, Role of oxygen vacancy in the plasma-treated TiO₂ photocatalyst with visible light activity for NO removal, *Journal of Molecular Catalysis A: Chemical*, 2000, **161**, 205–212.
- 21 N. Serpone, D. Lawless, and R. Khairutdinov, Size effects on the photophysical properties of colloidal anatase TiO₂ particles: Size quantization or direct transitions in this indirect semiconductor? *Journal of Physical Chemistry*, 1995, **99**, 16646–16654.
- 22 G. Liu, F. Li, D.-W. Wang, D.-M. Tang, C. Liu, X. Ma, G. Q. Lu, and H.-M. Cheng, Electron field emission of a nitrogen-doped TiO₂ nanotube array, *Nanotechnology*, 2008, **19**, 025606.
- 23 E. Scolan and C. Sanchez, Synthesis and Characterization of Surface-Protected Nanocrystalline Titania Particles, *Chemistry of Materials*, 1998, **10**, 3217–3223.
- 24 A. S. Attar, M. S. Ghamsari, F. Hajiesmaeilbaigi, and S. Mirdamadi, Modifier ligands effects on the synthesized TiO₂ nanocrystals, *Journal of Materials Science*, 2008, **43**, 1723–1729.
- 25 H. C. Choi, Y. M. Jung, and S. bin Kim, Size effects in the Raman spectra of TiO₂ nanoparticles, *Vib Spectrosc*, 2005, **37**, 33–38.
- 26 W. F. Zhang, Y. L. He, M. S. Zhang, Z. Yin, and Q. Chen, Raman scattering study on anatase TiO₂ nanocrystals, *Journal of Physics D: Applied Physics*, 2000, **33**, 912–916.
- 27 T. Cottre, M. Fingerle, M. Kranz, T. Mayer, B. Kaiser, and W. Jaegermann, Interaction of Water with Atomic Layer Deposited Titanium Dioxide on p-Si Photocathode: Modeling of Photoelectrochemical Interfaces in Ultrahigh Vacuum with Cryo-Photoelectron Spectroscopy, *Advanced Materials Interfaces*, DOI:10.1002/admi.202002257.
- 28 C. di Valentin and D. Fittipaldi, Hole scavenging by organic adsorbates on the TiO₂ surface: A DFT model study, *Journal of Physical Chemistry Letters*, 2013, **4**, 1901–1906.
- 29 J. Garcia-Amoros, U. Banin, M. Baroncini, and Y. Ben-Shahar, *Photoactive Semiconductor Nanocrystal Quantum Dots*, Springer International Publishing, Cham, 2017.
- 30 P. Y. Bruice, *Organic chemistry*, Pearson Education, Santa Barbara, 8th edition, 2016.

- 31 Y. Suda, T. Morimoto, and M. Nagao, Adsorption of Alcohols on Titanium Dioxide (Rutile) Surface, *Langmuir*, 1987, **3**, 99–104.
- 32 R. Battino, *Oxygen and ozone*, Pergamon Press, 1981, vol. 7.
- 33 A. Rahimi Niaraki, M. R. Saraei, F. Kazemi, and B. Kaboudin, Chemoselective photocatalytic oxidation of alcohols to aldehydes and ketones by nitromethane on titanium dioxide under violet 400 nm LED light irradiation, *Organic and Biomolecular Chemistry*, 2020, **18**, 2326–2330.
- 34 C. Han, M. Y. Qi, Z. R. Tang, J. Gong, and Y. J. Xu, Gold nanorods-based hybrids with tailored structures for photoredox catalysis: fundamental science, materials design and applications, *Nano Today*, 2019, **27**, 48–72.
- 35 C. S. Enache, J. Schoonman, and R. V. A. N. D. E. Krol, The Photoresponse of Iron- and Carbon-Doped TiO₂ (Anatase) Photoelectrodes, 2004, **2**, 177–182.
- 36 U. Joost, A. Šutka, M. Oja, K. Smits, N. Döbelin, A. Loot, M. Järvekülg, M. Hirsimäki, M. Valden, and E. Nömmiste, Reversible Photodoping of TiO₂ Nanoparticles for Photochromic Applications, *Chemistry of Materials*, 2018, **30**, 8968–8974.
- 37 Y. Yan, M. Han, A. Konkin, T. Koppe, D. Wang, T. Andreu, G. Chen, U. Vetter, J. R. Morante, and P. Schaaf, Slightly hydrogenated TiO₂ with enhanced photocatalytic performance, *Journal of Materials Chemistry A*, 2014, **2**, 12708–12716.
- 38 Y. L. Chueh, C. H. Hsieh, M. T. Chang, L. J. Chou, C. S. Lao, J. H. Song, J. Y. Gan, and Z. L. Wang, RuO₂ nanowires and RuO₂/TiO₂ core/shell nanowires: From synthesis to mechanical, optical, electrical, and photoconductive properties, *Advanced Materials*, 2007, **19**, 143–149.
- 39 U. Joost, A. Šutka, M. Visnapuu, A. Tamm, M. Lembinen, M. Antsov, K. Utt, K. Smits, E. Nömmiste, and V. Kisand, Colorimetric gas detection by the varying thickness of a thin film of ultrasmall PTSA-coated TiO₂ nanoparticles on a Si substrate, *Beilstein Journal of Nanotechnology*, 2017, **8**, 229–236.
- 40 M. Knite, V. Teteris, A. Kiploka, and J. Kaupuzs, Polyisoprene-carbon black nanocomposites as tensile strain and pressure sensor materials, *Sensors and Actuators, A: Physical*, 2004, **110**, 142–149.
- 41 Y. Li, J. K. Cooper, W. Liu, C. M. Sutter-Fella, M. Amani, J. W. Beeman, A. Javey, J. W. Ager, Y. Liu, F. M. Toma, and I. D. Sharp, Defective TiO₂ with high photoconductive gain for efficient and stable planar heterojunction perovskite solar cells, *Nature Communications*, 2016, **7**, 1–7.
- 42 K. Maier, A. Helwig, G. Müller, P. Hille, and M. Eickhoff, Effect of water vapor and surface morphology on the low temperature response of metal oxide semiconductor gas sensors, *Materials*, 2015, **8**, 6570–6588.
- 43 G. Harrison, K. Katsiev, Y. Alsalik, G. Thornton, and H. Idriss, Switch in photocatalytic reaction selectivity: The effect of oxygen partial pressure on carbon-carbon bond dissociation over hydroxylated TiO₂(1 1 0) surfaces, *Journal of Catalysis*, 2018, **363**, 117–127.
- 44 X. Wei, G. Zhu, J. Fang, and J. Chen, Synthesis, Characterization, and Photocatalysis of Well-Dispersible Phase-Pure Anatase TiO₂ Nanoparticles.
- 45 H. Su, Y. T. Huang, Y. H. Chang, P. Zhai, N. Y. Hau, P. C. H. Cheung, W. T. Yeh, T. C. Wei, and S. P. Feng, The Synthesis of Nb-doped TiO₂ Nanoparticles for Improved-Performance Dye Sensitized Solar Cells, *Electrochimica Acta*, 2015, **182**, 230–237.

- 46 J. Yang, X. Zhang, C. Wang, P. Sun, L. Wang, B. Xia, and Y. Liu, Solar photocatalytic activities of porous Nb-doped TiO₂ microspheres prepared by ultrasonic spray pyrolysis, *Solid State Sciences*, 2012, **14**, 139–144.
- 47 S. Parthasarathy and V. Parthasarathi, A statistical study on the measurability of Bijvoet differences in crystals with type-I and type-II degree of centrosymmetry, *Acta Crystallographica Section A*, 1976, **32**, 768–771.
- 48 N. Yu, Y. Hu, X. Wang, G. Liu, Z. Wang, Z. Liu, Q. Tian, M. Zhu, X. Shi, and Z. Chen, Dynamically tuning near-infrared-induced photothermal performances of TiO₂ nanocrystals by Nb doping for imaging-guided photothermal therapy of tumors, *Nanoscale*, 2017, **9**, 9148–9159.
- 49 L. de Trizio, R. Buonsanti, A. M. Schimpf, A. Llordes, D. R. Gamelin, R. Simonutti, and D. J. Milliron, Nb-Doped Colloidal TiO₂ Nanocrystals with Tunable Infrared Absorption, *Chemistry of Materials*, 2013, **25**, 3383–3390.
- 50 C. J. Dahlgren, A. Agrawal, C. M. Staller, J. Adair, and D. J. Milliron, Anisotropic Origins of Localized Surface Plasmon Resonance in n-Type Anatase TiO₂ Nanocrystals, *Chemistry of Materials*, 2019, **31**, 502–511.
- 51 T. R. N. Kutty and M. Avudaijai, Sacrificial water photocleavage using Nb-doped TiO₂ fine particles under band gap irradiation, *International Journal of Hydrogen Energy*, 1990, **15**, 621–628.
- 52 A. E. Gekhman, V. M. Nekipelov, S. G. Sakharov, K. I. Zamaraev, and I. I. Moiseev, Mechanism of the oxidation of acetylacetone by hydrogen peroxide, catalyzed by Mo(VI) complexes, *Bulletin of the Academy of Sciences of the USSR Division of Chemical Science*, 1986, **35**, 1126–1130.
- 53 M. B. Browning, S. N. Cereceres, P. T. Luong, and E. M. Cosgriff-Hernandez, Determination of the in vivo degradation mechanism of PEGDA hydrogels, *Journal of Biomedical Materials Research – Part A*, 2014, **102**, 4244–4251.
- 54 G. Amato, E. Grasso, V. Longo, and P. G. Gervasi, Oxidation of N, N-dimethylformamide and N, N-diethylformamide by human liver microsomes and human recombinant P450s, *Toxicology Letters*, 2001, **124**, 11–19.
- 55 C. Joyce-Pruden, J. K. Pross, and Y. Li, Photoinduced reduction of aldehydes on titanium dioxide, *The Journal of Organic Chemistry*, 1992, **57**, 5087–5091.
- 56 S. Kohtani and H. Miyabe, in *Titanium Dioxide*, ed. J. Brown, Nova Science Publishers, 2014.
- 57 S. Kohtani, E. Yoshioka, K. Saito, A. Kudo, and H. Miyabe, Photocatalytic hydrogenation of acetophenone derivatives and diaryl ketones on polycrystalline titanium dioxide, *Catalysis Communications*, 2010, **11**, 1049–1053.
- 58 Y. Hu and W. Pan, Calculation of pore scattering in transparent ceramics, *Solid State Phenomena*, 2018, **281 SSP**, 655–660.
- 59 J. G. J. Peelen and R. Metselaar, Light scattering by pores in polycrystalline materials: Transmission properties of alumina, *Journal of Applied Physics*, 1974, **45**, 216–220.



Raivis Eglītis was born in 1993 in Riga. He received a Bachelor's degree in Chemical Engineering in 2016 and a Master's degree in Material Nanotechnologies in 2018 from Riga Technical University. Since 2016, he has been a research assistant with Riga Technical University. Currently, he is a researcher with the Institute of Materials and Surface Engineering of the Faculty of Materials Science and Applied Chemistry of Riga Technical University. His research interests include spectroscopy as well as the optical properties of materials.